1   # Sigmoidal Water Retention Function with Improved Behavior in Dry

2   # and Wet Soils

3

4   Gerrit Huibert de Rooij, Juliane Mai, and Raneem Madi

5

6   G.H. de Rooij and R. Madi, Helmholtz Centre for Environmental Research – UFZ GmbH, Soil

7   System Science Dept., Theodor–Lieser–Strasse 4, 06120 Halle (Saale), Germany; R. Madi,

8   current address: GFI Grundwasser–Consulting–Institut GmbH, Meraner Strasse 10, 01217

9   Dresden, Germany.

10   J. Mai, University of Waterloo, Dept. Civil and Environmental Engineering, 200 University

11   Ave West, Waterloo, ON N2L 3G1, Canada.

12

13   Corresponding author: G.H. de Rooij (gerrit.derooij@ufz.de)

Abstract

14

15

16 A popular parameterized soil water retention curve (SWRC) has a hydraulic conductivity

17 curve associated with it that can have a physically unacceptable infinite slope at saturation.

18 The problem was eliminated before by giving the SWRC a non–zero air–entry value. This

19 improved version still has an asymptote at the dry end, which limits its usefulness for dry

20 conditions and causes its integral to diverge for commonly occurring parameter values. We

21 therefore joined the parameterizations' sigmoid mid–section to a logarithmic dry section

22 ending at zero water content for a finite matric potential, as was done previously for a

23 power–law type SWRC. We selected five SWRC parameterizations that had been proven to

24 produce unproblematic near–saturation conductivities and fitted these and our new curve

25 to data from 21 soils. The logarithmic dry branch gave more realistic extrapolations into the

26 dry end of both the retention and the conductivity curves than an asymptotic dry branch.

27 We tested the original curve, its first improvement, and our second improvement by feeding

28 them into a numerical model that calculated evapotranspiration and deep drainage for nine

29 combinations of soils and climates. The new curve was more robust than the other two. The

30 new curve was better able to produce a conductivity curve with a substantial drop during

31 the early stages of drying than the earlier improvement. It therefore generated smaller

32 amounts of more evenly distributed deep drainage compared to the spiked response to

33 rainfall produced by the earlier improvement.

Introduction

The soil water retention function introduced by van Genuchten (1980) has been the most popular parameterization (denoted VGN below; these and other abbreviations are listed in Appendix A) to describe the SWRC in numerical models for unsaturated flow for the past few decades (e.g., Kroes et al., 2017; Šimůnek and Bradford, 2008; Šimůnek et al., 2016):

$$\theta(h) = \theta_r + (\theta_s - \theta_r)(1 + |\alpha h|^n)^{\frac{1}{n}-1}, \quad h \leq 0 \tag{1}$$

where h denotes the matric potential in equivalent water column [L]. The volumetric water content is denoted by θ, with the subscript 's' denoting its value at saturation and the subscript 'r' its residual, or irreducible, value. Parameters α [L^{-1}] and n are shape parameters.

Van Genuchten (1980) combined Eq. (1) with Mualem's (1976) conductivity model and derived an analytical expression for the unsaturated hydraulic conductivity curve:

$$K(h) = K_s \frac{\left[1 - |\alpha h|^{n-1}(1 + |\alpha h|^n)^{\frac{1}{n}-1}\right]^2}{(1 + |\alpha h|^n)^{\frac{1}{2}-\frac{1}{2n}}} \tag{2}$$

where K [LT^{-1}] is the soil hydraulic conductivity and K_s [LT^{-1}] its value at saturation.

Hysteretic (Kool and Parker, 1987) and multimodal versions (Durner, 1994) of Eq. (1) are available. Apart from the convenience of having analytical expressions for the retention as well as the conductivity curve, the function's popularity derives from its

3

56   continuous derivative and its inflection point, which gives it considerable flexibility in

57   fitting observations.

58   Fuentes et al. (1991) warned that the asymptotic residual water content at the dry

59   end could lead to a non–converging integral of the retention curve when the integration is

60   carried out between the saturated water content and a water content that approximates the

61   residual water content in the limit. In that case, the area below the retention curve becomes

62   infinite. Fuentes et al. (1991) showed that this would lead to an unlimited amount of water

63   stored in a column of a finite length at hydrostatic equilibrium if its height was such that the

64   residual water content was approximated closely at the top of the column. This physically

65   impossible case is only avoided if $n > 2$ in Eq. (1), a condition which is often not satisfied.

66   Near saturation, the slope $\mathrm{d}\theta/\mathrm{d}h$ is not zero at zero matric potential. This implies

67   that the soil has pores that have at least one infinite principal radius according to the

68   Laplace–Young Law (Hillel, 1998, p. 46), which is physically unacceptable (see also Iden et

69   al., 2015). Durner (1994) noted this could lead to an infinite slope in the hydraulic

70   conductivity function of Mualem (1976) when the matric potential approached zero, and

71   Ippisch et al. (2006) showed that if $n < 2$ this would indeed be the case. The more recent

72   sigmoid curve of Fredlund and Xing (1994) and its modification by Wang et al. (2016), used

73   by Wang et al. (2018) and Rudiyanto et al. (2020) have the same problem (see Appendix B

74   for the proof). The curve of Assouline et al. (1998) is based on the Weibull distribution, and

75   therefore has a non–zero slope at zero matric potential when its fitting parameter η is

76   smaller than 2, which was the case for 75% of the soils for which it was fitted. None of these

77   curves therefore offers a remedy to the problem associated with VGN.

78   Corrections for the conductivity curve were proposed by Vogel et al. (2001), Schaap

79   and van Genuchten (2006), and Iden et al. (2015), but these leave the effect of the non–

80   physical, very large pores on the SWRC intact and create an inconsistency between the

81   retention model and the conductivity model. For instance, Iden et al. (2015) clipped the

82   integral in the conductivity function at a matric potential h_c somewhat below zero. In the

83   range between h_c and zero, their modified unsaturated hydraulic conductivity increased

84   linearly with the water content (Iden et al. (2015), Fig. 1), which is not physically realistic

85   because the pore sizes that are being filled are increasing in size according to Eq. (1) or its

86   multimodal version (Peters et al., 2011). Only Ippisch et al. (2006) addressed the

87   underlying problem in the SWRC by introducing a non–zero air–entry value, thereby

88   eliminating excessively large pores whilst maintaining the mathematical consistency

89   between the expressions for the retention and the conductivity curves. In doing so they

90   sacrificed the continuity of the derivative of the VGN curve. Iden et al. (2015) suspected this

91   would pose a challenge to numerical solves of Richards' equation, but Ippisch et al.'s (2006)

92   numerical simulations ran without difficulty. Their equation scaled the sigmoid curve by its

93   value at the air–entry value h_{ae} [L] and introduced a saturated section for $h > h_{ae}$.

94

95    $$\theta(h) = \begin{cases} \theta_r + (\theta_s - \theta_r)\left(\dfrac{1+|\alpha h|^n}{1+|\alpha h_{ae}|^n}\right)^{\frac{1}{n}-1}, & h \leq h_{ae} \\ \theta_s, & h > h_{ae} \end{cases} \qquad (3)$$

96

97   This function is denoted VGA below.

98   The smooth, sigmoidal shape of VGN resembles many observed curves for which the

99   data points in the wet range were obtained by equilibrating vertically placed cylindrical soil

100   samples at well–defined matric potentials and determining the corresponding water

101   content by weighing the sample (Klute, 1986, p. 644–647). Liu and Dane (1995) took into

102   account the vertical variation of the water content in such samples and demonstrated that a

103   power–law SWRC with a well–defined air–entry matric value but without inflection point

104   can produce a sigmoid–type apparent SWRC if the non–uniform distribution of water in the

105   sample is ignored. A series of data points suggesting a smooth SWRC therefore does not

106   intrinsically contradict the existence of a discrete non–zero air–entry value, corroborating

107   the correction to VGN by Ippisch et al. (2006).

108   Madi et al. (2018) generalized the analysis of Ippisch et al. (2006) and applied it to

109   18 parameterizations of the SWRC to verify that the slope of the hydraulic conductivity near

110   saturation would remain finite. Apart from Eq. (3), only the expressions developed by

111   Brooks and Corey (1964) (denoted BCO), Fayer and Simmons (1995) (denoted FSB), and

112   the junction model of Rossi and Nimmo (1994) (denoted RNA) satisfied this requirement.

113   In the latter case, a modification that smoothed the curve near saturation needed to be

114   removed. All these equations have a power law relationship between the water content and

115   the matric potential, and therefore do not have the sigmoid shape of VGN and VGA.

116   In a separate development, several researchers argued that in the dry range, water is

117   bound to the soil by adsorptive rather than capillary forces. Usually, a logarithmic term that

118   allowed the adsorbed water content to go to zero at a prescribed matric potential was

119   added to a capillary term. The former would dominate in the dry range and become

120   negligible as the soil became wetter (e.g., Campbell and Shiozawa, 1992; Fayer and

121   Simmons, 1995; Khlosi et al., 2006; Peters, 2013). The logarithmic relationship was based

122   on the sorption theory of Bradley (1936). It removed the asymptote and the associated

123   problem of the non–converging integral of the SWRC that Fuentes et al. (1991) warned

124   about. Rossi and Nimmo (1994) presented a junction model in which a critical matric

125   potential separated purely capillary bound water from solely adsorbed water. The

126   modified junction model of Rossi and Nimmo (1994) is

127

128
$$\theta(h) = \begin{cases} \theta_s \beta \, ln\left(\frac{h_d}{h}\right), & h_d \leq h \leq h_j \\ \theta_s \left(\frac{h_0}{h}\right)^\lambda, & h_j \leq h \leq h_i \\ \theta_s \left[1 - c\left(\frac{h}{h_0}\right)^2\right], & h_i \leq h \leq 0 \end{cases} \tag{4}$$

129

130   The first (dry) branch is logarithmic, with h_d [L] the matric potential at which the water

131   content reaches zero, and β a shape parameter. The middle branch is the power law

132   adopted from Brooks and Corey (1964) (without smoothing near saturation), where λ is a

133   shape parameter and h_0 [L] is a fitting parameter. The final (wet) branch is a parabolic

134   correction to avoid a discontinuity in the derivative at the air-entry value, with parameter c

135   a function of λ and h_0 (Hutson and Cass, 1987). Madi et al. (2018) pointed out that this

136   correction puts such strict constraints on the parameters of the conductivity curve that the

137   usual models are ruled out. The first and middle branch are joined at h_j [L], the middle and

138   final branch at h_i [L]. Rossi and Nimmo (1994) reduced the number of fitting parameters by

139   requiring that the water contents and the first derivatives of the branches match at at h_j and

140   h_i. This junction model avoids the problem of many of the other models that would have

141   some capillary bound water still present in the soil below the matric potential at which the

142   adsorbed water content had gone to zero.

143   As noted above, the introduction of a non–zero air–entry value by Ippisch et al.

144   (2006) eliminated the unphysically large slopes of the hydraulic conductivity according to

145   Mualem (1976). The approach of Rossi and Nimmo (1994) resolved the issue of the

146   asymptotic behavior in the dry range. The objective of this paper therefore is to combine

147   Rossi and Nimmo's (1994) model for the dry range with the VGA model of Ippisch et al.

148   (2006) to arrive at a SWRC (denoted RIA) that has a non–zero air–entry value, a sigmoid

149   shape in the intermediate range, a dry branch that can reach zero water content at a finite

150   matric potential, and therefore a finite integral. We will also develop a closed-form

151   expression for the unsaturated hydraulic conductivity based on this SWRC. For

152   completeness, a generalized expression for multimodal SWRCs will also be derived.

153   Together with the other functions that lead to physically acceptable behavior of the

154   hydraulic conductivity near saturation (BCO, FSB, RNA, and VGA), RIA will be fitted to 21

155   soils selected from the UNSODA database (National Agricultural Library, 2017; Nemes et al.,

156   2001) that cover a wide range of textures (Madi et al., 2018). For comparison VGN is also

157   included, in view of its de facto status as the standard parameterization for the SWRC. All

158   three versions with the sigmoid shape (VGN, VGA, and RIA) will be tested in a simulation

159   study for different combinations of soil types and climates.

160

Theory

161

The Soil Water Retention Curve

162

163   The junction model of Rossi and Nimmo (1994) has a SWRC with a logarithmic dry

164   branch without residual water content. The parameterization proposed by Ippisch et al.

165   (2006) combines the sigmoid shape of van Genuchten (1980) with a non–zero air–entry

166   value. By setting the θ_r in Ippisch et al. (2006) to zero, we can combine the two models to

167   give the following parameterization:

168

169    $$\theta(h) = \begin{cases} 0, & h \leq h_d \\ \theta_s \beta \ln\left(\frac{h_d}{h}\right), & h_d < h \leq h_j \\ \theta_s \left(\frac{1+|\alpha h|^n}{1+|\alpha h_{ae}|^n}\right)^{\frac{1}{n}-1}, & h_j < h \leq h_{ae} \\ \theta_s, & h > h_{ae} \end{cases} \tag{5}$$

170

171   where subscripts 'd' and 'ae' denote the value at which the water content reaches zero and

172   the air–entry value, respectively, and subscript 'j' indicates the value at which the

173   logarithmic and sigmoid branch are joined. The first branch ensures that no water can be

174   present at matric potentials below h_d. The second, logarithmic, branch is identical to that of

175   Eq. (4). The third, sigmoidal, branch between h_j and h_{ae}, and the fourth branch, for matric

176   potentials larger than the air-entry value, are from Eq. (3). Joining instead of adding the

177   logarithmic and the sigmoid functions avoids potentially non-monotonic behavior (Peters

178   et al., 2011).

179   The derivative of Eq. (5) is

180

181    $$\frac{d\theta}{dh}(h) = \begin{cases} 0, & h \leq h_d \\ \frac{\theta_s \beta}{h}, & h_d < h \leq h_j \\ \theta_s \alpha(n-1)|\alpha h|^{n-1}(1+|\alpha h_{ae}|^n)^{1-\frac{1}{n}}(1+|\alpha h|^n)^{\frac{1}{n}-2}, & h_j < h \leq h_{ae} \\ 0, & h > h_{ae} \end{cases} \tag{6}$$

182

183   Mass continuity dictates that the SWRC is continuous. At the air–entry value, this condition

184   is met irrespective of the parameter values. At h_j, continuity requires the following equality

185   to hold:

186

187     $$\beta \ln\left(\frac{h_d}{h_j}\right) = \left(\frac{1+|\alpha h_j|^n}{1+|\alpha h_{ae}|^n}\right)^{\frac{1}{n}-1} \qquad (7)$$

188

189   In accordance with Rossi and Nimmo (1994) we also require the derivatives at h_j to match,

190   leading to

191

192     $$\beta = (n-1)|\alpha h_j|^n (1+|\alpha h_{ae}|^n)^{1-\frac{1}{n}}\left(1+\left|\alpha h_j\right|^n\right)^{\frac{1}{n}-2} \qquad (8)$$

193

194   Combining Eqs. (7) and (8) and solving for h_d gives:

195

196     $$h_d = h_j \exp\left(\frac{1+|\alpha h_j|^{-n}}{n-1}\right) \qquad (9)$$

197

198   This leaves h_{ae}, h_j, θ_s, α, and n as fitting parameters.

199   The derivation of a multimodal curve analogous to that of Durner (1994) and

200   Zurmühl and Durner (1998) is straightforward if the values of h_{ae} and h_j are kept the same

201   for all contributing terms:

202
$$\theta(h) = \begin{cases} 0, & h \leq h_{\mathrm{d}} \\ \theta_{\mathrm{s}}\beta\ln\left(\frac{h_{\mathrm{d}}}{h}\right), & h_{\mathrm{d}} < h \leq h_{\mathrm{j}} \\ \theta_{\mathrm{s}} \sum_{i=1}^{k} w_i \left(\frac{1+|\alpha_i h|^{n_i}}{1+|\alpha_i h_{\mathrm{ae}}|^{n_i}}\right)^{\frac{1}{n_i}-1}, & h_{\mathrm{j}} < h \leq h_{\mathrm{ae}} \\ \theta_{\mathrm{s}}, & h > h_{\mathrm{ae}} \end{cases} \qquad (10)$$

203

204   where the modality is indicated by k. The weighting factors w_i are bounded on the interval

205   [0,1] and their sum must equal 1 (Durner, 1994; Zurmühl and Durner, 1998). Requiring the

206   logarithmic and the multimodal branch as well as their derivatives to match at h_{j} leads to

207

208    $$\beta = \sum_{i=1}^{k} w_i (n_i - 1)|\alpha_i h_{\mathrm{j}}|^{n_i} (1 + |\alpha_i h_{\mathrm{ae}}|^{n_i})^{1-\frac{1}{n_i}} \left(1 + |\alpha_i h_{\mathrm{j}}|^{n_i}\right)^{\frac{1}{n_i}-2} \qquad (11)$$

209

210   and

211

212    $$h_{\mathrm{d}} = h_{\mathrm{j}} \exp\left[\frac{\sum_{i=1}^{k} w_i (1+|\alpha_i h_{\mathrm{ae}}|^{n_i})^{1-\frac{1}{n_i}}\left(1+|\alpha_i h_{\mathrm{j}}|^{n_i}\right)^{\frac{1}{n_i}-1}}{\sum_{i=1}^{k} w_i (n_i-1)|\alpha_i h_{\mathrm{j}}|^{n_i}(1+|\alpha_i h_{\mathrm{ae}}|^{n_i})^{1-\frac{1}{n_i}}\left(1+|\alpha_i h_{\mathrm{j}}|^{n_i}\right)^{\frac{1}{n_i}-2}} \right] \qquad (12)$$

213

214   The fitting parameters are h_{ae}, h_{j}, θ_{s}, α_i, n_i, and w_i.

215

216   **The Unsaturated Hydraulic Conductivity Curve**

217   The primary focus of this paper is on the SWRC. Nevertheless, it is worthwhile to

218   find a closed-form expression for the unsaturated hydraulic conductivity that can be used in

219   association with Eq. (5). Kosugi (1999) proposed the following conductivity model (see

220   also Ippisch et al., 2006):

221

$$K(h) = K\big(h(S_e)\big) = \begin{cases} K_s S_e^\tau \left(\dfrac{\int_{-\infty}^{h(S_e)} |h|^{-\kappa} \frac{dS}{dh} dh}{\int_{-\infty}^{h_{ae}} |h|^{-\kappa} \frac{dS}{dh} dh} \right)^\gamma, & h < h_{ae} \\ K_s, & h \geq h_{ae} \end{cases} \qquad (13)$$

223

224   with γ, κ, and τ denoting shape parameters, S_e denoting the degree of saturation $(\theta - \theta_r)/(\theta_s$

225    $- \theta_r)$, and S representing a variable running over all values of the degree of saturation from

226   zero to its actual value S_e. Mualem's (1976) conductivity model is a special case of Eq. (13),

227   with $\gamma = 2$, $\kappa = 1$, and $\tau = 0.5$. Madi et al. (2018) give parameter combinations for additional

228   models.

229   The integrals in Eq. (13) that arise when Eq. (6) is used to find dS/dh can be

230   evaluated analytically if $\kappa = 1$. The resulting conductivity function is

231

$$K(h) = \begin{cases} 0, & h \leq h_d \\[2em] K_s \left(\beta \ln \left| \dfrac{h_d}{h} \right| \right)^\tau \left[\dfrac{\dfrac{\beta}{|h_d|} - \dfrac{\beta}{|h|}}{\dfrac{\beta}{|h_d|} - \dfrac{\beta}{|h_j|} + \dfrac{|\alpha h_{ae}|^n}{|h_{ae}|} - (1+|\alpha h_{ae}|^n)^{1-\frac{1}{n}} F(h_j)} \right]^\gamma, & h_d < h \leq h_j \\[3em] K_s \left(\dfrac{1+|\alpha h|^n}{1+|\alpha h_{ae}|^n} \right)^{\frac{\tau}{n}-\tau} \left\{ \dfrac{\dfrac{\beta}{|h_d|} - \dfrac{\beta}{|h_j|} + (1+|\alpha h_{ae}|^n)^{1-\frac{1}{n}} [F(h) - F(h_j)]}{\dfrac{\beta}{|h_d|} - \dfrac{\beta}{|h_j|} + \dfrac{|\alpha h_{ae}|^n}{|h_{ae}|} - (1+|\alpha h_{ae}|^n)^{1-\frac{1}{n}} F(h_j)} \right\}^\gamma, & \\[1em] & h_j < h \leq h_{ae} \\[2em] K_s, & h > h_{ae} \end{cases}$$

233   (14a)

234

12

235   where

236

237    $$F(h) = \frac{|\alpha h|^n (1+|\alpha h|^n)^{\frac{1}{n}-1}}{|h|}$$ (14b)

238

239   If only the hydraulic conductivity at saturation is available, one can use the values

240   for α and n of the water retention curve and fix parameters γ and τ according to one of

241   several conductivity models (Madi et al., 2018) to define an unsaturated hydraulic

242   conductivity curve, but this is not recommended. It is better to have additional data points

243   of the hydraulic conductivity curve so that parameters γ and τ, and perhaps even

244   conductivity-specific values of α and n, can be fitted directly to the conductivity data.

245   Equations (14a) and (14b) have the advantage that they can be expressed in closed

246   form but they do not account for non-capillary flow in dry soils, vapor flow, or sequences of

247   evaporation and condensation in soils with pockets of water and soil air. Hence, they are of

248   limited value for water flows in dry soils. For such conditions more sophisticated

249   conductivity could be selected, for instance using the framework presented by Weber et al.

250   (2019).

251   The conductivity function associated with the multimodal soil water retention

252   function cannot be expressed in closed form. For that case, the degree of saturation for any

253   h can be found with Eq. (10) and the corresponding hydraulic conductivity determined with

254   Eq. (13) or another conductivity model.

255

256   **Materials and Methods**

13

257   We selected 21 soils from the UNSODA database that had sufficient retention data

258   and together covered the textures represented in UNSODA. We then fitted Eq. (5) to these

259   soils using a Shuffled Complex Evolution algorithm (see Madi et al. (2018) and Appendix C

260   for details of the algorithm and the fitting procedure). We slightly modified the fitting code

261   used by Madi et al. (2018) to generate output that can more readily be converted to the

262   MATER.IN input file for Hydrus–1D, the numerical model used in this study. We therefore

263   refitted BCO, FSB, RNA, VGN, and VGA as well.

264   One–dimensional simulations for all combinations of three soils and three climates

265   were carried out to examine how the choice of parameterization affected fluxes at the soil

266   surface and in the subsoil. The model Hydrus–1D version 4.16.0110 (Šimůnek et al., 2013,

267   PC-progress website) was used for this purpose. The selected soils were a loamy sand

268   (UNSODA identifier: 2104), a silty loam (3261), and a clay (1181). Weather records were

269   generated from climate parameters based on weather data from Colombo (Sri Lanka,

270   monsoon climate), Tamale (Ghana, semi–arid climate), and Ukkel (Belgium, temperate

271   climate). Table 1 gives the most relevant statistics of the weather records. In order to

272   highlight the effects of the air–entry value and the logarithmic dry end of the SWRC, we

273   used the sigmoidal VGN, VGA, and RIA parameterizations in the simulations. The

274   Supplement details the generation of the weather records, the set–up of the simulations,

275   and the simulation results.

276

277   Table 1. Average cumulative monthly and annual rainfall and potential evapotranspiration

278   of the three test climates calculated from 1000–year generated weather records.

Month	Monsoon		Semi–arid		Temperate	
	Rain (mm)	ET_{pot} (mm)	Rain (mm)	ET_{pot} (mm)	Rain (mm)	ET_{pot} (mm)
Jan	94.0	160.5	14.3	159.4	69.0	12.7
Feb	83.3	156.0	12.9	158.1	55.6	18.8
Mar	217.6	166.8	13.7	185.0	59.4	34.4
Apr	233.8	160.0	34.1	177.7	57.1	51.1
May	237.4	164.0	117.6	166.6	24.5	73.9
Jun	138.5	164.7	140.9	151.4	24.4	83.3
Jul	139.4	172.4	141.8	153.2	23.2	86.3
Aug	137.1	174.4	213.5	145.0	20.9	73.7
Sep	133.0	164.7	214.7	136.9	23.8	50.6
Oct	325.8	142.3	76.6	154.1	38.0	30.8
Nov	328.8	128.1	12.9	149.3	49.1	16.1
Dec	112.0	150.9	12.9	151.9	51.2	11.2
Annual sum	2180.5	1904.8	1005.8	1888.7	496.1	542.9

279

280

281
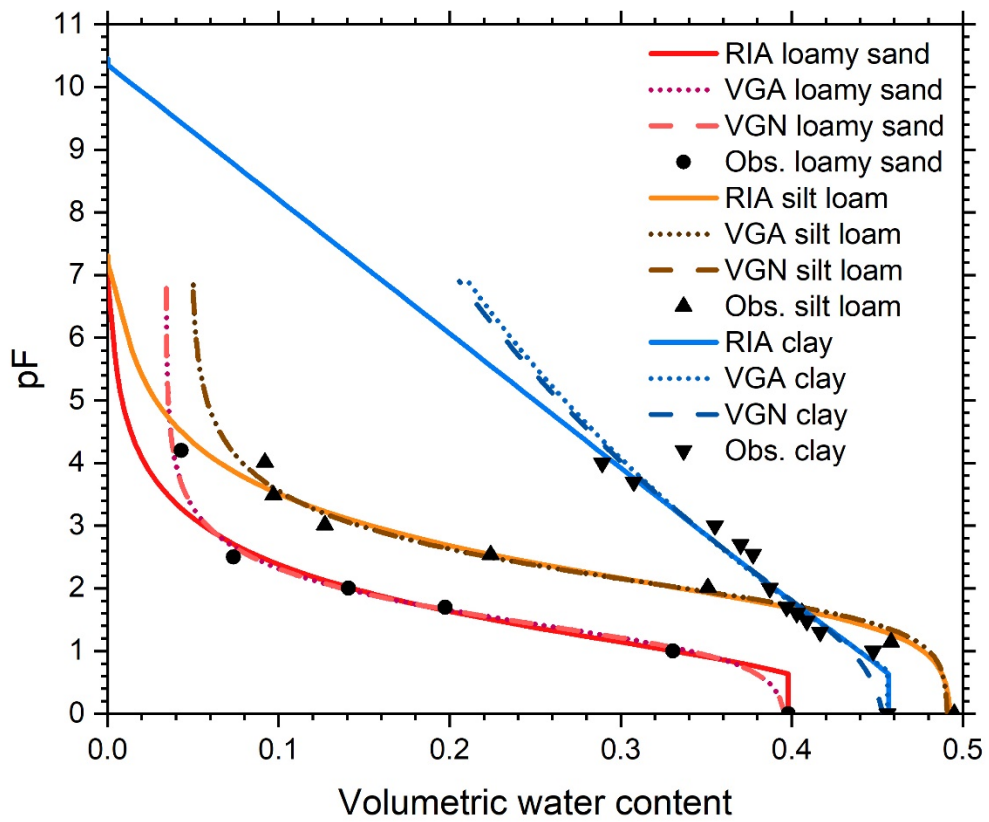
Figure 1. Soil water retention data of the soils used in the numerical simulations, and the retention curves fitted to these data for three parameterizations with a sigmoid midsection of the curve: the original model by van Genuchten (1980) (VGN), the modification thereof by Ippisch et al. (2006) (VGA), and the further modification introduced in this paper (RIA).

The different parameterizations of the SWRCs (Table 2, Fig. 1) were used to generate tables of the soil water retention and conductivity curves that were provided as input to Hydrus–1D. Equations (14a) and (14b) with $\gamma = 2$ and $\tau = 0.5$ (Mualem, 1976) were used to generate relative hydraulic conductivities (scaled by K_s). These were converted to unscaled

292 conductivities (Fig. 2) by multiplying with the K_s–value according to the UNSODA database,

293 and then included in the tables.

294

295 Table 2. Parameters of the fit to data of the three parameterizations of the soil water

296 retention curve used for the numerical simulations.

Soil	Parameter	θ_r	θ_s	α (cm^{-1})	n	h_{ae} (cm)	h_j (cm)
Clay	RIA	–	0.45666	0.70200	1.0543	−4.2523	−205.65
	VGA	2.12×10^{-6}	0.45603	1.7047	1.0543	−4.8324	–
	VGN	3.34×10^{-6}	0.45616	0.14265	1.0571	–	–
Silt	RIA	–	0.49346	0.023340	1.3691	-2.361×10^{-3}	-1.0739×10^6
loam	VGA	0.048871	0.49122	0.018365	1.5158	-2.081×10^{-3}	–
	VGN	0.048816	0.49134	0.018425	1.5149	–	–
Loamy	RIA	–	0.39801	0.17096	1.4106	−4.3581	-7.7464×10^5
sand	VGA	0.034209	0.39771	0.069661	1.6395	−0.016234	–
	VGN	0.034133	0.39772	0.069707	1.6389	–	–

297

298

299   For the clay soil, the recorded value (178 cm d^{-1}) was such that it can be assumed

300 that macropore flow contributed to its value. We therefore also ran simulations with a K_s –

301 value of 1.25 cm d^{-1}. This value was adopted from soil 1182 from the UNSODA database,

302 from the same location.

303

304
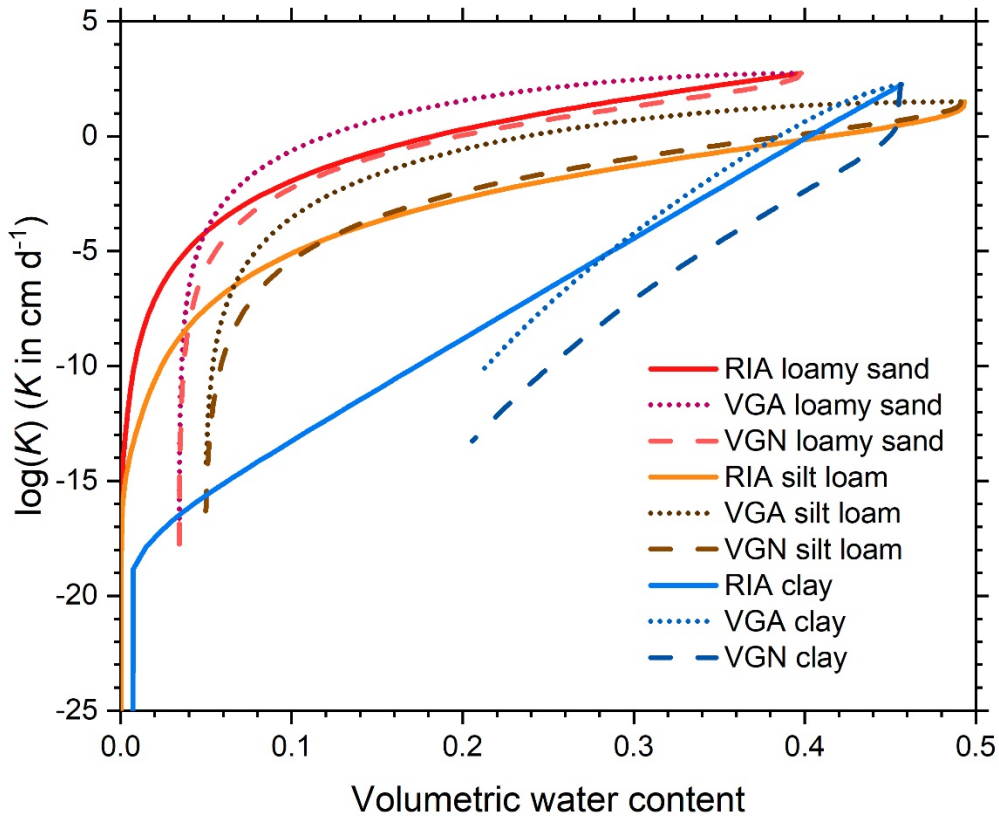
Figure 2. The unsaturated soil hydraulic conductivity curves derived from the fitted

retention curves depicted in Fig.1 and scaled by soil–specific values of the hydraulic

conductivity at saturation.

308

Results and Discussion

Fitted Curves for 21 Soils

The fitted parameter values (Tables C1–C4) and the associated curves (Figs. C2–C5)

are presented in Appendix C. The extra parameter of RIA compared to RNA and FSB gives it

a clear advantage in fitting the full water content range. The sigmoid shape of RIA provides

314   a better fit near the air entry value while still providing good fits of the drier data points

315   (e.g. 1121 in Fig. C3, all soils in Figs. C4–C5). In the wet range, the sigmoid curves (VGN,

316   VGA, RIA) outperform the power–law curves (BCO, FSB, RNA). In almost all cases, VGA and

317   RIA look very similar. Figure C3 shows multimodality in the data for five out of six soils that

318   cannot be reproduced by any of the parameterizations.

319   Many of the UNSODA soils have one retention data point at saturation and the next

320   at $h = -10$ cm. The air–entry value of many sandy soils is within that range. The fitting

321   routine struggles to fit h_{ae} to these data for VGA and RIA because the sigmoid shape of the

322   van Genuchten parameterization has such flexibility that it can fit the intermediate range

323   well for a range of h_{ae}–values. We therefore recommend making $\theta(h)$–measurements at one

324   or two matric potentials between zero and -10 cm for coarse–textured soils.

325   Eleven of the 21 soils have residual water contents for VGN and/or VGA that exceed

326   0.05 (up to 0.263), mostly in loamy sands, loams, and clays (Tables C1–C4). All of these and

327   several others have dry–end data points with water contents that appear too high (Figs. C2–

328   C5). These water contents may have been overestimated due to the lack of equilibrium

329   reported by Bittelli and Flury (2009). The parameterizations without asymptote (FSB, RNA,

330   RIA) generally have more plausible fits based on visual inspection of the graphs, but

331   because they do not follow the upward tail of the data in the dry end, their RMSE values for

332   the cases with suspicious dry–end data points are larger than those of VGN and VGA (Tables

333   C5–C8).

334   Especially for fine–textured soils, the lack of data points for air dryness or oven

335   dryness (Figs. C3–C5) causes the fitting procedure to treat θ_r for the asymptotic dry

336   branches and h_d for the logarithmic dry branches as pure fitting parameters for the drier

337   range of the data. This range exceeds pF4.2 in only one case and in several cases likely

338   suffers from lack of equilibrium (Bittelli and Flury, 2009). This leads to unrealistically high

339   values for both in many cases. If applications are envisioned for which low water contents

340   are expected, it would be better to have some data in the dry range and ensure equilibrium

341   has been achieved before fitting RIA.

342   We tested this on the data of Bittelli and Flury (2009) for undisturbed samples taken

343   at 0.15 m depth. We fitted RIA, VGA, and VGN with θ_s fixed at 0.45 to their pressure plate

344   data (which were unreliable in the dry range) and a combination of pressure plate data for

345   matric potentials larger than –1000 cm H_2O (pF3.0) and dew point data for higher pF

346   values (Table 3). Figure 3 shows that all three parameterizations gave good fits for both

347   data sets, and that the dry-end data points affect the entire SWRC. It is important to note

348   that the pF value of h_d for the combination of pressure plate and dew point data equals

349   6.428, close to the oven-dry value of pF6.8 approximated by most sample-drying ovens

350   according to Schneider and Goss (2012).

351   If reliable data in the dry range are not available but a realistic fit in the dry range is

352   necessary, one could add a virtual data point with zero water content at pF6.8 according to

353   Schneider and Goss (2012) and give it a high weight to force the fitting algorithm to

354   approximate it closely. We did not do so here to be able to observe how the various

355   parameterizations perform on frequently reported data ranges.

356   Figure C5 showcases a peculiarity of FSB. The original version by Fayer and

357   Simmons (1995) allowed capillary bound water to be present even if the adsorbed water

358   content was down to zero. We adopted the correction by Madi et al. (2018, Eq. (S12a)) that

359   forced the amount of water bound by capillary forces to zero if the adsorbed water content

20

360 reaches zero at pF6.8. In the case of clay soils, the parameter values are such that a

361 substantial amount of capillary bound water is still present at pF6.8, leading to a sudden

362 cut–off at pF6.8.

363

364 Table 3. Parameters of the fit to the pressure plate data and a combination of pressure plate

365 and dew point data of Bittelli and Flury (2009).

Data	Parameter	θ_r	θ_s	α (cm^{-1})	n	h_{ae} (cm)	h_j (cm)
Pressure plate	RIA	–	0.45000	0.019088	1.1479	-1.072×10^{-4}	-47876
	VGA	2.21×10^{-5}	0.45000	0.019091	1.1479	-3.105×10^{-3}	–
	VGN	6.76×10^{-7}	0.45000	0.019124	1.1478	–	–
Pressure plate (pF < 3) and dew point (pF ≥ 3)	RIA	–	0.45000	7.1162×10^{-3}	1.3041	-1.063×10^{-3}	-99989
	VGA	5.08×10^{-6}	0.45000	7.0471×10^{-3}	1.3056	-4.249×10^{-3}	–
	VGN	1.37×10^{-6}	0.45000	7.0448×10^{-3}	1.3053	–	–

366

367
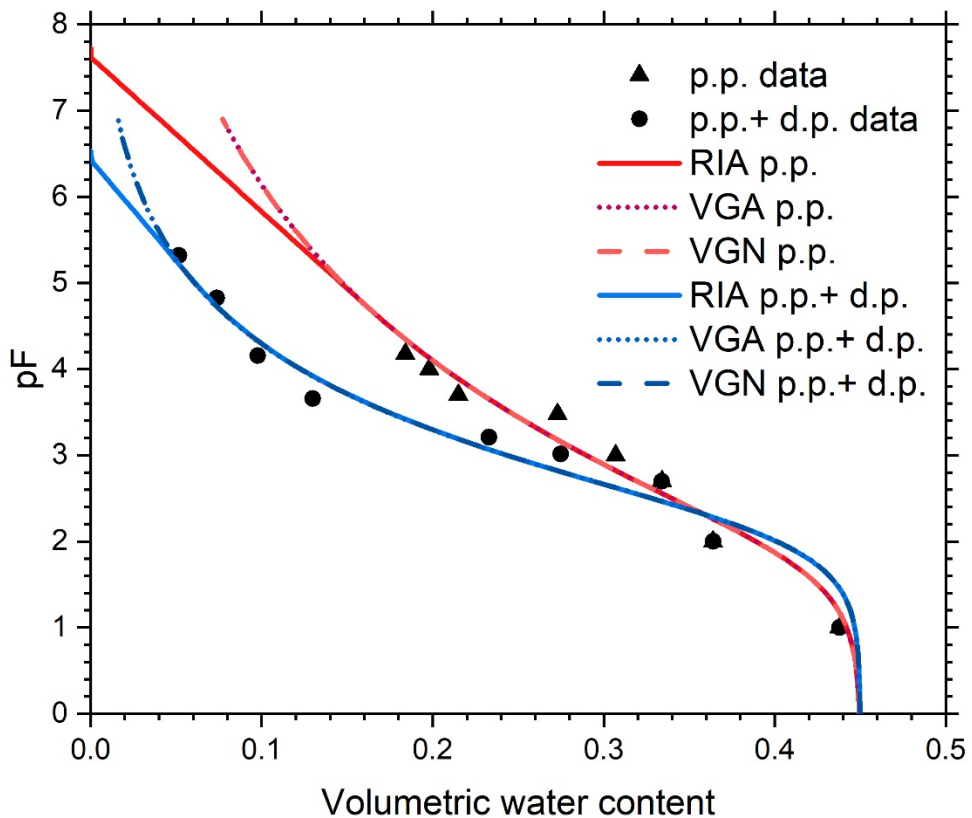
Figure 3. Soil water retention data obtained by Bittelli and Flury (2009) from samples placed on pressure plates (p.p. data) or from a combination of pressure plates for the wettest three data points and dew point measurements for the driest six data points (p.p. + d.p. data). The curves show the fits of the soil water retention curves according to van Genuchten (1989) (VGN), Ippisch et al. (2006) (VGA), and Eq. (5) (RIA).

The hydraulic conductivity curves based on water retention curve parameters and K_s very poorly match the data in most cases (Fig. C6–C9), which confirms that it is better to fit conductivity parameters to conductivity data instead of relying on values prescribed by theoretical models. We note here that all but one (soil 4450, Fig. C8) sets of unsaturated

379   conductivity data were obtained in the field, while all retention data were laboratory data

380   on drying samples. The reported K_s–values were probably measured in a separate

381   experiment (possibly in the laboratory), in which case a mismatch between K_s and the

382   unsaturated conductivity data is to be expected. The poor match with field data

383   notwithstanding, the graphs can be used to study the effect of the parameterization on the

384   shape of the $K(\theta)$ curve. The comparison between measured and modeled shapes of the

385   conductivity curves is inconclusive.

386   In many soils, regardless of texture, RIA's $K(\theta)$ curve drops of much slower in the

387   dry range than those of VGN and VGA (Fig. C6–C9), a consequence of the ability of the

388   underlying SWRC to reach zero water content at a finite matric potential. Near saturation,

389   RIA's $K(\theta)$ curve often drops off sharply before leveling off, in stark contrast to that of VGA,

390   which remains high in the wet range. Given the similarity in the $\theta(h)$ curves of VGA and RIA,

391   the difference in their $K(\theta)$ curves is remarkable. RIA's $K(\theta)$ curve is the only one that can

392   drop off sharply near saturation, level out somewhat in the mid-range and drop ever more

393   sharply in the dry range. It is below many of the other curves in the wet and mid-range, and

394   above most of them in the dry range.

395   Peters et al. (2011) developed parameter constraints to ensure physically plausible

396   shapes of the SRWC and the conductivity curve. For FSB, the criterion for non-monotonicity

397   of the conductivity curve is not met for soil 4450 (Fig. C8), resulting in K increasing with

398   decreasing water content near saturation.

399

400   **Model Simulations**

401   In total, 21 out of 36 combinations of soil–climate–parameterization ran to

402   completion. Runoff did not occur in any of the successful model runs. Convergence was not

403   achieved for any of the runs for the clay soil with the reduced K_s–value. For the clay soil

404   with the high K_s–value, only RIA ran to completion. The discontinuity of the first derivative

405   at the air-entry value did not cause numerical problems. In fact, the replacement of any

406   parametric expression by a look-up table creates a discontinuity of the first derivative at

407   every point of the look-up table.

408   Table 4 lists the main mean annual fluxes calculated from the simulation study. The

409   median flux was produced by RIA for all combinations of soil and climate. The mean annual

410   actual transpiration between the three parameterizations differed by more than 10% from

411   the median only for the silt loam under a temperate climate. The actual evaporation only

412   deviated more than 10% for the loamy sand under a semi-arid climate. The amount of

413   water leaving the soil profile differed substantially between parameterizations for the semi-

414   arid and temperate climate, especially for VGA (20–46% deviation from the median).

415   The daily data revealed significant differences on smaller time scales that will be

416   relevant if reactive solute transport is of interest (see the Supplement). The fluxes

417   generated by the VGA parameterizations responded more quickly and strongly to the

418   rainfall signal, with VGN and RIA giving a more delayed and smooth response. The SWRCs

419   (Fig. 1) offer no explanation for this, but Fig. 2 shows that VGA's hydraulic conductivity in

420   the wet and intermediate water content range for all three soils is considerably higher than

421   that of VGN and RIA, except for clay, where it is only moderately higher than RIA's and

422   drops below RIA at a water content of 0.28. Thus, small differences between SWRCs can

423   have a significant influence on soil water flow simulations through the effect of their

424   parameters on the soil hydraulic conductivity curve, an effect that the reviews by Leij et al.

425   (1997) and Assouline and Or (2013) took into consideration to some degree, but was not

426   considered in several other studies that compared different parameterizations (e.g., Rossi

427   and Nimmo, 1994; Assouline et al., 1998; Cornelis et al., 2005; Khlosi et al., 2008).

428 Table 4. Average of the annual sums of the actual transpiration and evaporation, and of the

429 outflow across the lower boundary of the simulated soil profiles. The averages were

430 calculated for the final six years of the simulation periods. The values in parentheses are

431 scaled with respect to the corresponding value for RIA.

Climate	Soil	Actual transpiration (mm)			Actual evaporation (mm)			Downward flux at 2 m depth (mm)		
		RIA	VGA	VGN	RIA	VGA	VGN	RIA	VGA	VGN
Monsoon	clay	962	–	–	543	–	–	876	–	–
	silt loam	1114	1044 (0.94)	1112 (1.06)	541	554 (1.02)	534 (0.96)	711	763 (1.07)	718 (0.94)
	loamy sand	1037	976 (0.94)	1024 (1.05)	480	440 (0.92)	461 (1.05)	863	959 (1.11)	896 (0.93)
Semi–arid	clay	585	–	–	319	–	–	294	–	–
	silt loam	657	588 (0.90)	653 (1.11)	297	303 (1.02)	287 (0.95)	164	226 (1.37)	177 (0.78)
	loamy sand	585	540 (0.92)	572 (1.06)	248	222 (0.89)	234 (1.06)	290	363 (1.25)	319 (0.88)
Temperate	clay	202	–	–	163	–	–	167	–	–
	silt loam	281	236 (0.84)	271 (1.15)	150	151 (1.01)	143 (0.95)	99	144 (1.46)	114 (0.79)
	loamy sand	224	205 (0.92)	214 (1.04)	130	118 (0.91)	124 (1.05)	174	208 (1.20)	190 (0.91)

432

Summary and Conclusions

433

434   The improvements incorporated in the RIA parameterization for the first time

435   remove problems of the popular VGN model in both the wet and the dry range while

436   retaining the desirable sigmoid shape in the mid–range. This shape allows its multimodal

437   version to represent SWRCs with multiple humps. RIA offers a wider range of shapes for the

438   conductivity curve than any other parameterization that does not lead to the unphysical

439   behavior near saturation that was revealed by Durner (1994) and Ippisch et al. (2006) for

440   VGN and by Madi et al. (2018) for 14 other parameterizations. RIA also proved to be more

441   robust during numerical simulations than VGN itself as well as its modification VGA, which

442   still has a non–physical asymptote at a non–zero residual water content. The deep drainage

443   generated by RIA was more spread out and smaller than the spiked response to rainfall

444   produced by VGA, probably because RIA was better able to produce a conductivity curve

445   with a substantial drop during the early stages of drying. We therefore hope that RIA or its

446   multimodal version will be adopted for use in numerical simulations of soil water flow. The

447   catalogue of parameters for 21 soils in Appendix C may be of help for such simulations.

Appendix A. List of Abbreviations

BC: Brooks and Corey (1964)

BCO: parameterization of the SWRC according to the original Brooks and Corey (1964)
equation

FSB: parameterization of the SWRC according to the BC–based version of Fayers and
Simmons (1995)

RIA: parameterization of the SWRC that combines RNA and VGA

RNA: parameterization of the SWRC according to the junction model of Rossi and Nimmo
(1994)

SWRC: soil water retention curve

RMSE: root mean square error

UNSODA: unsaturated soil hydraulic properties database

VGA: parameterization of the SWRC according to Ippisch et al. (2016)

VGN: parameterization of the SWRC according to the original van Genuchten (1980)
equation

Appendix B. Assessing the near-saturation behavior of recently developed soil water retention and hydraulic conductivity curves

Madi et al. (2018) developed a criterion that needs to be met to avoid unphysical behavior of the unsaturated soil hydraulic conductivity curve near saturation:

$$\lim_{h \uparrow 0} \left(|h|^{-\kappa} \frac{d\theta}{dh} \right) = 0 \tag{B1}$$

where κ is a fitting parameter (> 0) that appears in a several parameterizations of the unsaturated soil hydraulic conductivity curve based on the capillary bundle conceptualization.

Fredlund and Xing (1994) introduced the following parameterization for the soil water retention curve:

$$\theta(h) = \left[\frac{-\ln\left(1 + \frac{|h|}{|h_r|}\right)}{\ln\left(1 + \frac{b}{|h_r|}\right)} + 1 \right] \frac{\theta_s}{\left\{ \ln\left[e + \left(\frac{|h|}{a}\right)^n \right] \right\}^m} \tag{B2}$$

where the subscript 'r' denotes the value when the residual water content is reached, and a [L], n, and m are fitting parameters. The first term on the right-hand side is a correction term that forces the water content to zero for $h = -b$, with b equal to 10^7 cm (Fredlund and Xing, 1994) or 6.3×10^6 cm (Wang et al., 2016). Wang et al. (2016) also modified the correction factor to give

486

$$\theta(h) = \left[\frac{-\ln\left(1+\frac{c|h|}{|h_{\mathrm{r}}|}\right)}{\ln\left(1+\frac{bc}{|h_{\mathrm{r}}|}\right)}+1\right]\frac{\theta_s}{\left\{\ln\left[\mathrm{e}+\left(\frac{|h|}{a}\right)^n\right]\right\}^m} \tag{B3}$$

488

489 where c has to be small and positive. The derivative of Eq. (B3) is

490

$$\frac{\mathrm{d}\theta}{\mathrm{d}h} = \frac{-\theta_s}{\left\{\ln\left[\mathrm{e}+\left(\frac{|h|}{a}\right)^n\right]\right\}^m}\left\{\frac{mn|h|^{n-1}\left[\ln\left(1+\frac{bc}{|h_{\mathrm{r}}|}\right)\ln\left(1+\frac{c|h|}{|h_{\mathrm{r}}|}\right)-1\right]}{a^n\left[\mathrm{e}+\left(\frac{|h|}{a}\right)^n\right]\ln\left[\mathrm{e}+\left(\frac{|h|}{a}\right)^n\right]}-\frac{\ln\left(1+\frac{bc}{|h_{\mathrm{r}}|}\right)}{\frac{|h_{\mathrm{r}}|}{c}+|h|}\right\} \tag{B4}$$

492

493 The derivative of Eq. (B2) follows by setting c equal to 1 in Eq. (B4). Combining Eq.(B4)

494 with Eq. (B1) results in the following requirement:

495

$$\lim_{h\uparrow 0}\left[\frac{\theta_s mn}{\mathrm{e}a^n}|h|^{-\kappa+n-1}+\frac{c\theta_s\ln\left(1+\frac{bc}{|h_{\mathrm{r}}|}\right)}{|h_{\mathrm{r}}|}|h|^{-\kappa}\right]=0 \tag{B5}$$

497

498 The limit goes to zero if and only if the exponents in both terms are positive. Hence, $\kappa <$

499 $n-1$ and $\kappa < 0$. The first requirement may be met for some soils, but the second violates

500 the physical constraint that κ cannot be negative (Madi et al., 2018). Therefore, neither

501 Fredlund and Xing's (1994) nor Wang et al.'s (2016) parameterization lead to unsaturated

502 hydraulic conductivity curves that exhibit physically realistic behavior near saturation.

503 Wang et al. (2018) added a modification in the dry end of Wang et al. (2016), and

504 Rudiyanto et al. (2020) in turn used Wang et al.'s (2018) curves. Because the problem near

505 saturation was not resolved, these two hydraulic conductivity models suffer from the same

506 problem near saturation.

Appendix C. Fitted Parameters and Root Mean Square Error for Six Parameterizations of the Soil Water Retention Curve applied to Data of 21 Soils

510

The UNSODA soils selected for parameter fitting are grouped in Tables C1–C4 according to their texture classification according to Twarakavi et al. (2010). Sand is a major constituent of the mineral soil in Tables C1 and C2, silt in Table C3, and clay in Table C4. Figure C1 shows the textural composition of the soils. For each soil, the parameter values for six parameterizations are given, resulting in a total of 126 SWRC parameterizations. The Root Mean Square Errors (RMSE) for all fits are listed in Tables C5–C8. The saturated hydraulic conductivities of the soils as given by the UNSODA database are given in Table C9.

Madi et al. (2018) provide an analysis of the underlying functions of all parameterizations tested here, except RIA. The meaning of all variables except λ is explained in the main text. Variable λ is the power to which the factor (h / h_{ae}) is raised in the power–law segments of the SWRCs of BCO, FSB, and RNA. In RNA, λ is expressed as a function of the fitting parameters, and therefore does not appear in the tables.

The SWRCs defined by these parameterizations together with the data points on which they are based are given in Figs. C2–C5. The hydraulic conductivity curves according to Mualem (1976) that can be derived from the parameterizations (Eqs. (14a) and (14b) for RIA, equations for the other parameterizations in Madi et al. (2018)) are plotted in Figs. C6–C9. We plotted K as a function of θ because this relationship is less hysteretic than $K(h)$

529   (Koorevaar et al., 1983, p. 141) and some of the UNSODA data only provided $K(\theta)$ data

530   points. The conductivity data available in UNSODA are also plotted, but these were not used

531   to fit the curves to. The maximum pF value for which points on the curves were calculated

532   was set at 6.8 for VGN and VGA, and to the pF value corresponding to the fitted value of h_d

533   for RIA.

534   The comparison of theoretical conductivity curves based on water retention data

535   with the measured values showed a sometimes substantial deviation between hydraulic

536   conductivities measured at saturation and the K_s value used to create the theoretical curves.

537   The latter value was obtained by a query that made the database return a K_s value for the

538   soils that met all other criteria also included in the query. The conductivity data displayed

539   in the plots were separately obtained by requesting the database to return a report of

540   tabular data for each of the 21 soils. The reasons for the discrepancies between the queried

541   value and the tabulated may reflect separate experiments for measuring unsaturated and

542   saturated values of K.

543   There also are obvious differences between the water content at saturation between

544   the retention and the conductivity data. In all but one case (soil 4450, Fig. C8) the hydraulic

545   conductivity observations were made in the field whereas the retention data used were all

546   obtained from drying experiments in the laboratory. Scale differences, effects of air

547   enclosure and hysteresis in the field, and differences between different measurement

548   techniques explain these differences. We can therefore only compare the shape of the

549   theoretical curves with those of the data clouds.

32
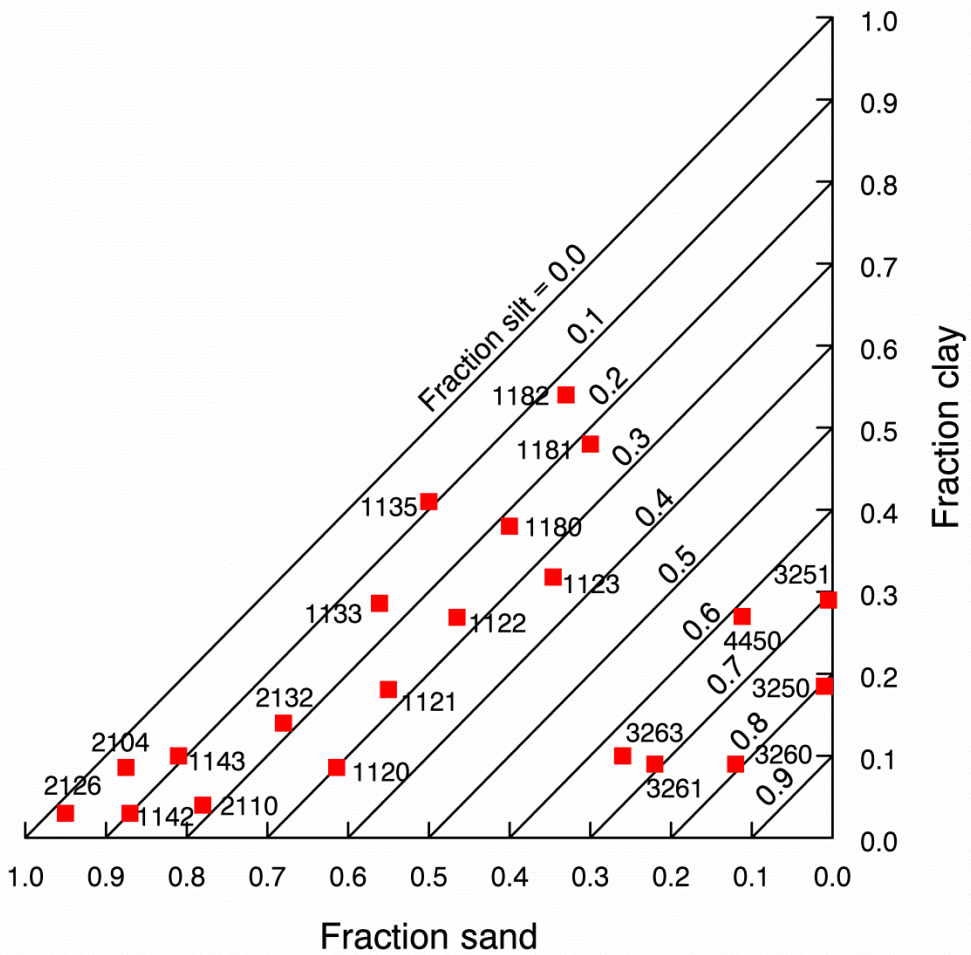
550

551 Figure C1. The positions in the texture triangle of the selected soils, indicated by their

552 UNSODA identifier. (Taken form Madi et al., 2018)

553

554   The RMSE was calculated from the weighted sum of squares of the differences

555   between calculated and observed water contents and pressure heads. The weights equaled

556   the estimated scaled standard deviations of the individual water retention observations

557   (pairs of matric potential and water content values). The standard deviations of the water

558   content observations were scaled to have an average value of 0.2. The scale factor needed to

559   arrive at this value was then applied to the standard deviations of the matric potential

560   values as well. This ensured that the weighting of water contents and matric potential

561   values was consistent with the original standard deviations of both. The scaling greatly

562   improved the efficiency of the parameter fitting procedure. The squared difference between

563   a single observed water content and its fitted value during a given iteration of the

564   parameter fitting algorithm, taking into account observation errors in both the water

565   content and the matric potential, is

566

567    $$\left(\frac{\theta_{\text{fit}} - \theta_{\text{obs}}}{\sigma_{\theta,\text{ scaled}} + \sigma_{h,\text{scaled}} \frac{d\theta}{dh}\big|_{h_{\text{obs}}}} \right)^2 \qquad\qquad (C1)$$

568

569   where $\sigma_{a,\text{ scaled}}$ is the scaled standard deviation of the variable a, subscript 'fit' signifies a

570   fitted value of the subscripted variable, and subscript 'obs' a measured value (Madi et al.,

571   2018). The slope of the SWRC in the denominator is estimated from the fitted

572   parameterization using the parameter values that have been fitted in the iteration that is

573   currently being tested.

574   The scale factors applied to the observation error standard deviations varied

575   between soils but not between parameterizations fitted to the same soil. RMSE values of

34

576 different parameterizations valid for a particular soil can therefore be readily compared.

577 Comparisons between soils only give a rough indication. When the water contents at which

578 measurements were taken differ strongly from one soil to another, the comparison of their

579 RMSE values is less reliable.

580   In case the measured water contents were obtained at hydrostatic equilibrium, the

581 fitted water content calculated directly from the matric potential could not be compared to

582 the observed water content. To approximate the soil sample on which the observation was

583 made, a hypothetical soil slab of the same height as the sample was divided into 20

584 horizontal layers. If UNSODA did not specify the sample height, it was assumed to be 5.0 cm.

585 The matric potential in the center of each layer was determined from the given matric

586 potential, which was assumed to apply to the center of the sample. The water content of the

587 soil slab was then calculated as the average water content of its 20 layers. This water

588 content was used to calculate the difference between the observed and the fitted water

589 content. Figure C10 shows a comparison of retention points calculated for three soils based

590 directly on the RIA parameterization and based on the same parameterization applied to a

591 hypothetical sample of 5.0 cm height at hydrostatic equilibrium with the nominal matric

592 potential valid at the sample center. Deviations are small, even for the loamy sand.

593 Table C1. The fitting parameters and their values for six parameterizations for sandy soils in the A1

594 and A2 classifications of Twarakavi et al. (2010) from the UNSODA database (National Agricultural

595 Library, 2017; Nemes et al., 2001). The three–character parameterization label is explained in the

596 main text.

Parameterization	Parameter	Unit	Soil (UNSODA identifier and classification according to Twarakavi et al. (2010))		
			2126 A1	1142 A2	2104 A2
BCO	θ_r	–	1.63E–2	4.92E–5	2.27E–2
	θ_s	–	0.377	0.250	0.398
	h_{ae}	cm	−6.78	−7.00	−6.79
	λ	–	0.846	0.210	0.434
FSB	θ_s	–	0.377	0.250	0.398
	θ_a	–	2.58E–2	6.26E–5	5.46E–2
	h_{ae}	cm	−6.76	−7.00	−6.73
	λ	–	0.861	0.211	0.468
RNA	θ_s	–	0.378	0.250	0.398
	h_{ae}	cm	−6.37	−7.00	−6.17
	h_j	cm	−8.87E4	−9.24E4	−6.45E4
	h_d	cm	−3.60E5	−1.07E7	−9.73E5
VGN	θ_r	–	3.39E–2	9.42E–2	3.41E–2
	θ_s	–	0.376	0.242	0.398
	α	cm^{-1}	6.85E–2	1.99E–2	6.97E–2
	n	–	2.73	2.93	1.64
VGA	θ_r	–	3.39E–2	9.64E–2	3.42E–2
	θ_s	–	0.376	0.242	0.398
	α	cm^{-1}	6.84E–2	1.98E–2	6.97E–2
	n	–	2.73	3.05	1.64
	h_{ae}	cm	−0.101	−0.240	−1.62E–2
RIA	θ_s	–	0.378	0.245	0.398
	α	cm^{-1}	0.239	2.68E–2	0.171
	n	–	1.77	1.47	1.41
	h_{ae}	cm	−5.82	−7.00	−4.36
	h_j	cm	−1.76E6	−4.35E5	−7.75E5

597

598 Table C2. The fitting parameters and their values for six parameterizations for sandy soils in the A3

599 and A4 classifications of Twarakavi et al. (2010) from the UNSODA database (National Agricultural

600 Library, 2017; Nemes et al., 2001). The three–character parameterization label is explained in the

601 main text.

Para–meteri–zation	Parameeter	Unit	Soil (UNSODA identifier and classification according to Twarakavi et al. (2010))					
			1120 A3	1143 A3	2110 A3	2132 A3	1121 A4	1133 A4
BCO	θ_r	–	6.15E–6	2.71E–5	0.103	4.10E–5	2.64E–5	5.37E–5
	θ_s	–	0.311	0.279	0.348	0.303	0.350	0.330
	h_{ae}	cm	−10.0	−7.00	−25.5	−8.00	−10.0	−206
	λ	–	0.204	0.169	0.537	0.107	0.118	0.103
FSB	θ_s	–	0.311	0.279	0.348	0.308	0.346	0.330
	θ_a	–	4.33E–5	4.26E–4	0.213	0.298	0.324	0.310
	h_{ae}	cm	−10.0	−7.00	−25.7	−3.24	−10.0	−206
	λ	–	0.204	0.169	0.763	0.422	0.377	0.213
RNA	θ_s	–	0.311	0.279	0.351	0.303	0.352	0.330
	h_{ae}	cm	−10.0	−7.00	−20.3	−8.00	−10.0	−220
	h_j	cm	−7.32E4	−8.46E4	−6.44E4	−7.18E4	−8.73E4	−6.77E4
	h_d	cm	−9.95E6	−3.18E7	−2.35E6	−8.06E8	−3.88E8	−8.68E8
VGN	θ_r	–	7.22E–2	9.24E–2	0.126	1.25E–4	1.70E–5	0.202
	θ_s	–	0.305	0.278	0.360	0.305	0.339	0.324
	α	cm^{-1}	1.72E–2	4.66E–2	2.63E–2	5.73E–2	7.21E–3	7.34E–4
	n	–	1.69	1.49	1.84	1.14	1.26	3.02
VGA	θ_r	–	7.37E–2	0.112	0.106	6.61E–4	1.47E–5	0.202
	θ_s	–	0.303	0.276	0.348	0.306	0.339	0.324
	α	cm^{-1}	1.72E–2	4.41E–2	0.230	6.06E–2	7.16E–3	7.35E–4
	n	–	1.71	1.66	1.56	1.14	1.27	3.00
	h_{ae}	cm	−9.37	−6.81	−25.3	−8.47E–4	−2.73E–2	−12.5
RIA	θ_s	–	0.308	0.280	0.360	0.306	0.339	0.328
	α	cm^{-1}	3.01E–2	6.39E–2	4.18E–2	6.08E–2	7.13E–2	1.30E–3
	n	–	1.29	1.23	1.33	1.14	1.27	1.20
	h_{ae}	cm	−1.24E–3	−4.96E–4	−7.85	−7.44E–4	−9.11E–4	−220
	h_j	cm	−1.71E6	−7.01E6	−9.37E6	−7.81E6	−2.04E6	−5.07E6

602 Table C3. The fitting parameters and their values for six parameterizations for silty soils from the

603 UNSODA database (National Agricultural Library, 2017; Nemes et al., 2001). The three–character

604 parameterization label is explained in the main text.

			Soil (UNSODA identifier and classification according to Twarakavi et al. (2010))					
			3260 B2	3261 B2	3263 B2	3250 B4	3251 B4	4450 B4
Para–meteri–zation	Parameter	Unit						
BCO	θ_r	–	2.85E–6	3.42E–6	3.85E–7	3.85E–6	1.94E–6	2.77E–5
	θ_s	–	0.470	0.499	0.460	0.540	0.500	0.380
	h_{ae}	cm	−28.6	−13.5	−28.8	−30.5	−18.2	−4.80
	λ	–	0.281	0.256	0.255	0.183	9.56E–2	9.51E–2
FSB	θ_s	–	0.470	0.499	0.460	0.540	0.500	0.380
	θ_a	–	1.33E–5	6.49E–5	1.33E–5	0.173	0.431	0.320
	h_{ae}	cm	−28.6	−13.5	−28.8	−30.0	−10.9	−0.882
	λ	–	0.281	0.256	0.255	0.241	0.197	0.196
RNA	θ_s	–	0.470	0.499	0.460	0.540	0.500	0.380
	h_{ae}	cm	−28.6	−13.5	−28.8	−30.5	−18.2	−4.81
	h_j	cm	−9.23E4	−9.43E4	−7.48E4	−7.87E4	−1.97E4	−2.63E4
	h_d	cm	−3.23E6	−4.96E6	−3.75E6	−6.86E6	−7.66E8	−9.69E8
VGN	θ_r	–	5.25E–2	4.88E–2	4.48E–2	3.10E–2	1.60E–5	1.16E–6
	θ_s	–	0.472	0.491	0.461	0.540	0.501	0.379
	α	cm^{-1}	1.62E–2	1.84E–2	1.53E–2	1.21E–2	2.62E–2	0.164
	n	–	1.47	1.51	1.41	1.28	1.11	1.10
VGA	θ_r	–	5.27E–2	4.89E–2	6.12E–2	3.80E–4	7.21E–5	2.80E–5
	θ_s	–	0.472	0.491	0.457	0.540	0.500	0.379
	α	cm^{-1}	1.62E–2	1.84E–2	1.49E–2	1.33E–2	3.66E–2	1.26
	n	–	1.47	1.52	1.46	1.25	1.11	1.10
	h_{ae}	cm	−3.26E–3	−2.08E–3	−15.1	−4.87	−7.31	−4.54
RIA	θ_s	–	0.474	0.493	0.463	0.540	0.500	0.379
	α	cm^{-1}	2.04E–2	2.33E–2	1.86E–2	1.33E–2	3.57E–2	0.164
	n	–	1.33	1.37	1.31	1.25	1.11	1.10
	h_{ae}	cm	−5.95E–3	−2.36E–3	−2.43E–3	−4.80	−7.12	−1.21E–3
	h_j	cm	−1.49E6	−1.07E6	−8.62E6	−8.02E6	−8.33E6	−9.89E6

605

Table C4. The fitting parameters and their values for six parameterizations for clayey soils from the UNSODA database (National Agricultural Library, 2017; Nemes et al., 2001). The three–character parameterization label is explained in the main text.

Para–meteri–zation	Para–meter	Unit	Soil (UNSODA identifier and classification according to Twarakavi et al. (2010))					
			1135 C2	1182 C2	1122 C4	1123 C4	1180 C4	1181 C4
BCO	θ_r	–	3.94E–4	1.79E–4	2.64E–4	2.13E–4	5.22E–4	1.24E–5
	θ_s	–	0.420	0.549	0.362	0.358	0.497	0.456
	h_{ae}	cm	−106	−0.977	−10.0	−10.0	−11.1	−5.17
	λ	–	7.85E–2	4.41E–2	3.37E–2	2.69E–2	5.65E–2	5.40E–2
FSB	θ_s	–	0.420	0.548	0.360	0.356	0.495	0.456
	θ_a	–	0.400	0.307	0.350	0.340	0.491	0.345
	h_{ae}	cm	−106	−0.230	−5.75	−10.0	−8.58	−13.2
	λ	–	0.172	5.64E–2	6.60E–2	5.69E–2	100	8.08E–2
RNA	θ_s	–	0.420	0.549	0.370	0.370	0.497	0.456
	h_{ae}	cm	−106	−3.61	−9.99	−9.99	−0.150	−7.66
	h_j	cm	−107	−12.2	−10.5	−10.7	−24.1	−22.1
	h_d	cm	−1.64E8	−1.00E9	−1.00E9	−1.00E9	−1.00E9	−1.00E9
VGN	θ_r	–	0.263	8.94E–6	1.16E–4	0.210	0.255	3.34E–6
	θ_s	–	0.413	0.548	0.359	0.354	0.496	0.456
	α	cm^{-1}	1.02E–3	0.753	1.37E–2	2.92E–3	0.805	0.143
	n	–	2.37	1.05	1.05	1.21	1.26	1.06
VGA	θ_r	–	0.263	1.19E–5	5.78E–2	0.188	2.63E–2	2.12E–6
	θ_s	–	0.413	0.548	0.359	0.354	0.498	0.456
	α	cm^{-1}	1.02E–3	1.21	1.37E–2	3.22E–3	10.1	1.70
	n	–	2.37	1.05	1.07	1.17	1.06	1.05
	h_{ae}	cm	−1.03	−0.467	−4.18E–2	−10.0	−1.11E–2	−4.83
RIA	θ_s	–	0.416	0.548	0.359	0.354	0.497	0.457
	α	cm^{-1}	1.86E–3	1.31	1.39E–2	4.00E–3	14.2	0.702
	n	–	1.16	1.05	1.05	1.06	1.06	1.05
	h_{ae}	cm	−106	−0.525	−3.80E–3	−9.99	−4.41E–2	−4.25
	h_j	cm	−7.57E6	−9.97E6	−9.56E4	−4.43E6	−415	−206

610   Table C5. Root mean square errors of the parameter fits for the sandy or loamy soils (A1 and A2

611   soils according to Twarakavi et al., 2010)

Parameterization	Soil (UNSODA identifier and classification according to Twarakavi et al. (2010))		
	2126 A1	1142 A2	2104 A2
BCO	0.0620	0.0990	0.0481
FSB	0.0626	0.0990	0.0517
RNA	0.0659	0.0989	0.0553
VGN	0.0330	0.0252	0.0278
VGA	0.0330	0.0250	0.0278
RIA	0.0652	0.0504	0.0542

612

613

614   Table C6. Root mean square errors of the parameter fits for the sandy soils (A3 and A4 soils

615   according to Twarakavi et al., 2010)

Parameterization	Soil (UNSODA identifier and classification according to Twarakavi et al. (2010))					
	1120	1143	2110	2132	1121	1133
	A3	A3	A3	A3	A4	A4
BCO	0.0926	0.0501	0.0445	0.0356	0.1288	0.0803
FSB	0.0926	0.0500	0.0445	0.0292	0.1054	0.0700
RNA	0.0926	0.0500	0.0457	0.0356	0.1286	0.0775
VGN	0.0446	0.0333	0.0378	0.0204	0.0720	0.0175
VGA	0.0489	0.0396	0.0445	0.0203	0.0720	0.0175
RIA	0.0643	0.0346	0.0491	0.0203	0.0720	0.0530

616

617

Table C7. Root mean square errors of the parameter fits for the silty soils.

| Parameterization | Soil (UNSODA identifier and classification according to Twarakavi et al. (2010)) | | | | | |
| | 3260 | 3261 | 3263 | 3250 | 3251 | 4450 |
	B2	B2	B2	B4	B4	B4
BCO	0.0793	0.1316	0.0973	0.0822	0.0551	0.0499
FSB	0.0794	0.1316	0.0973	0.0815	0.0395	0.0445
RNA	0.0793	0.1316	0.0973	0.0822	0.0551	0.0499
VGN	0.0456	0.0607	0.0638	0.0413	0.0474	0.0485
VGA	0.0455	0.0607	0.0769	0.0412	0.0466	0.0497
RIA	0.0543	0.0698	0.0668	0.0412	0.0466	0.0485

619

620

621   Table C8. Root mean square errors of the parameter fits for the clayey soils.

| Parameterization | Soil (UNSODA identifier and classification according to Twarakavi et al. (2010)) | | | | | |
| | 1135 | 1182 | 1122 | 1123 | 1180 | 1181 |
	C2	C2	C4	C4	C4	C4
BCO	0.0913	0.0494	0.0349	0.0489	0.0187	0.0428
FSB	0.0721	0.0441	0.0212	0.0321	0.1196	0.0360
RNA	0.0812	0.0913	0.1235	0.1501	0.0347	0.0570
VGN	0.0208	0.0488	0.0197	0.0244	0.0411	0.0433
VGA	0.0208	0.0485	0.0198	0.0243	0.0197	0.0429
RIA	0.0519	0.0485	0.0197	0.0244	0.0180	0.0391

622

623

624   Table C9. Values for the hydraulic conductivity at saturation (K_s) for the selected soils from

625   the UNSODA database. The soils are identified by their UNSODA identifier. Their classification

626   according to Twarakavi et al. (2010) is also given.

UNSODA identifier	Texture classification	K_s (cm d^{-1})
2126	A1	1.10E3
1142	A2	13.4
2104	A2	553
1120	A3	37.9
1143	A3	23.5
2110	A3	16.3
2132	A3	5.52
1121	A4	7.13
1133	A4	7.13
3260	B2	10.8
3261	B2	32.0
3263	B2	54.0
3250	B4	1.51
3251	B4	2.74
4450	B4	1.20
1135	C2	0.142
1182	C2	1.25
1122	C4	2.92
1123	C4	0.740
1180	C4	215
1181	C4	178

627

628
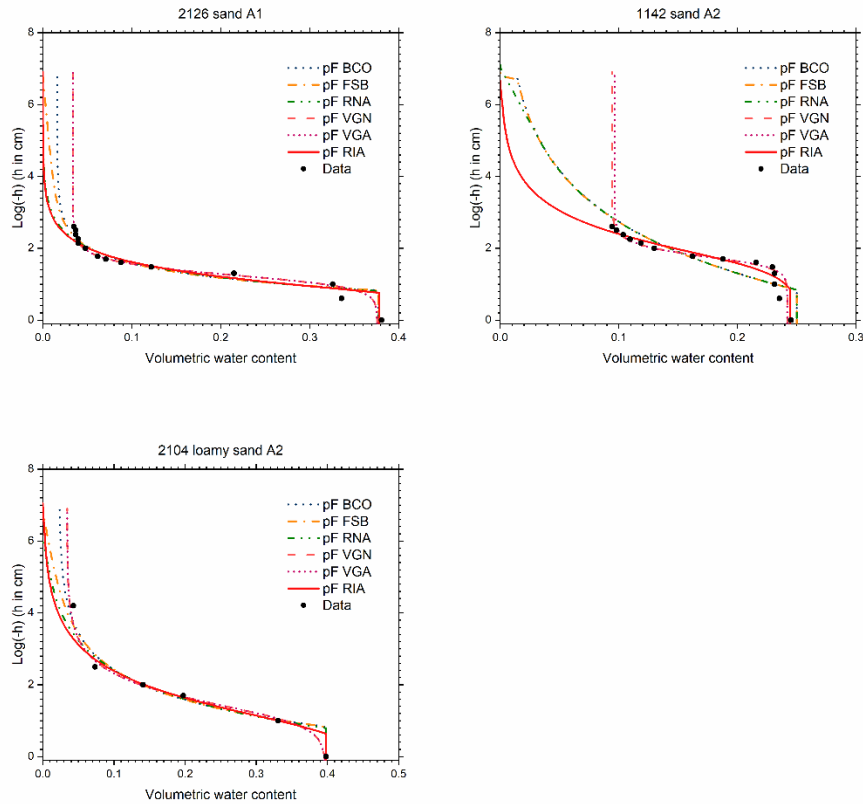
Figure C2. Retention data and fitted soil water retention curves according to six

parameterizations for selected UNSODA soils with Twarakavi et al.'s (2010) A1 or A2

classification. The parameterizations are explained in the text.

632
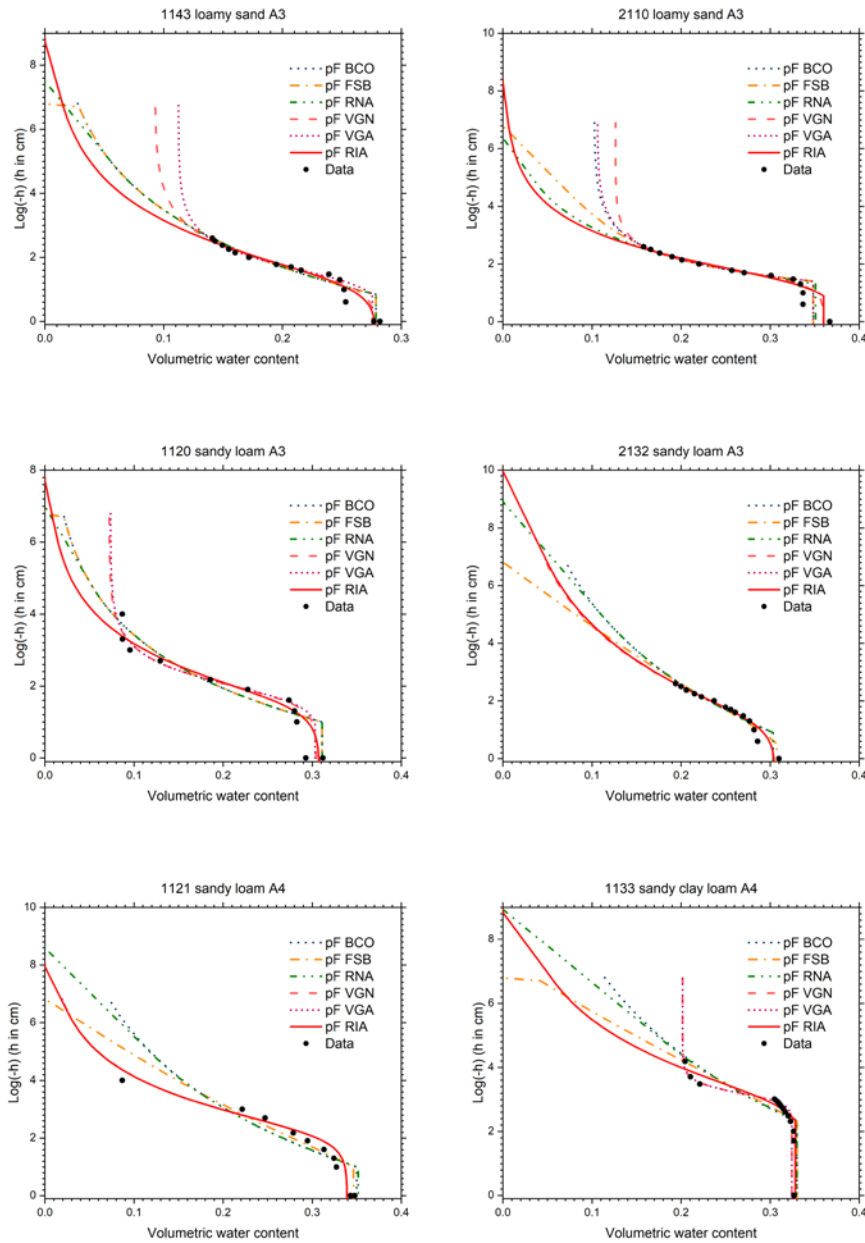
Figure C3. Retention data and fitted soil water retention curves according to six

parameterizations for selected UNSODA soils with Twarakavi et al.'s (2010) A3 or A4

classification. The parameterizations are explained in the text.

636
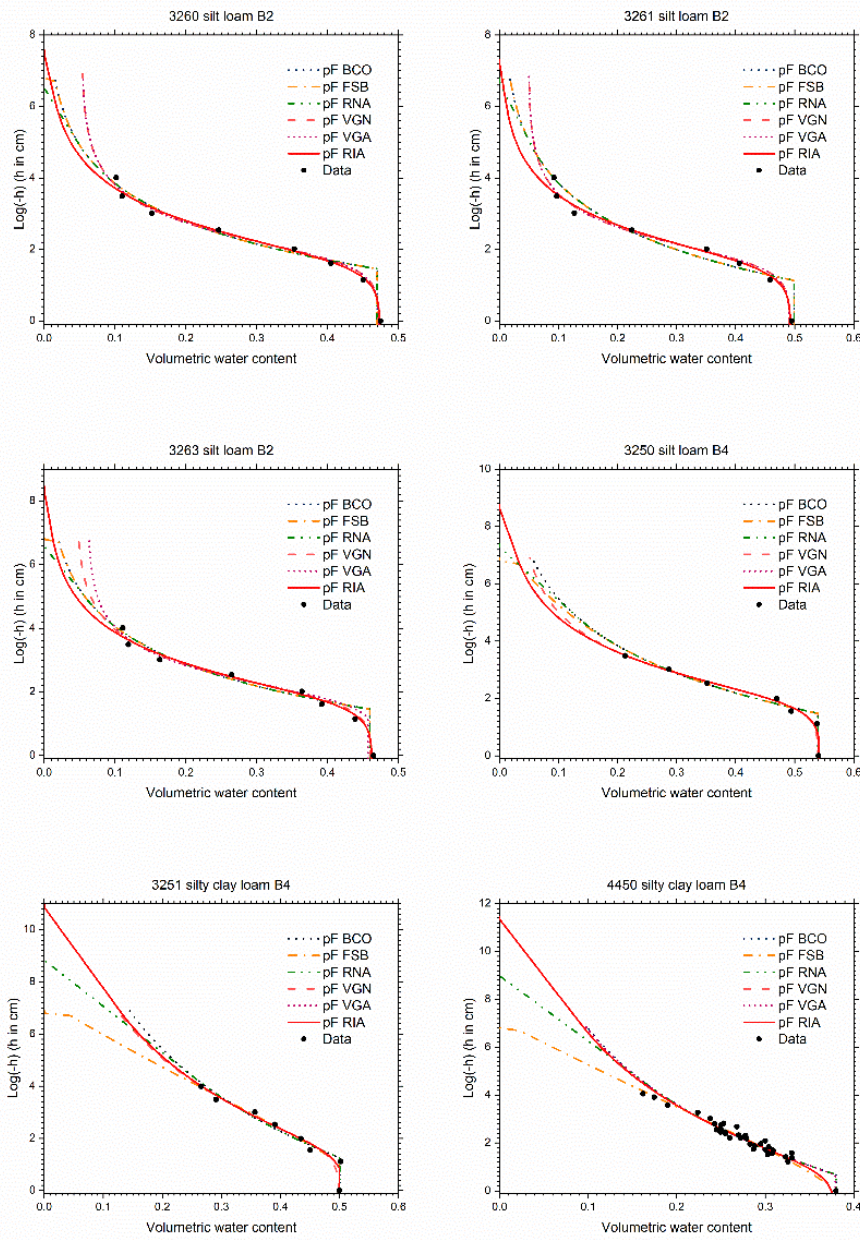
Figure C4. Retention data and fitted soil water retention curves according to six

parameterizations for selected UNSODA soils with Twarakavi et al.'s (2010) B2 or B4

classification. The parameterizations are explained in the text.

640
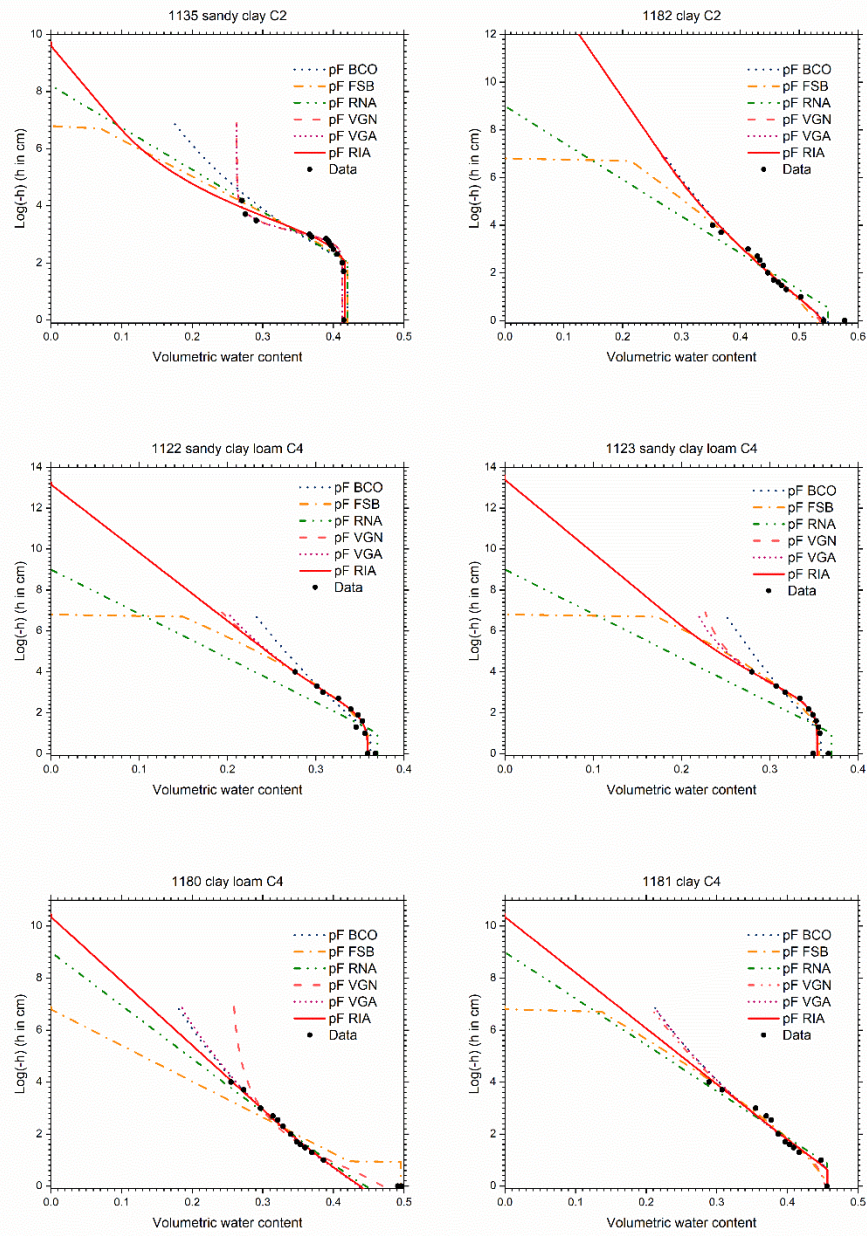
Figure C5. Retention data and fitted soil water retention curves according to six

parameterizations for selected UNSODA soils with Twarakavi et al.'s (2010) C2 or C4

classification. The parameterizations are explained in the text.
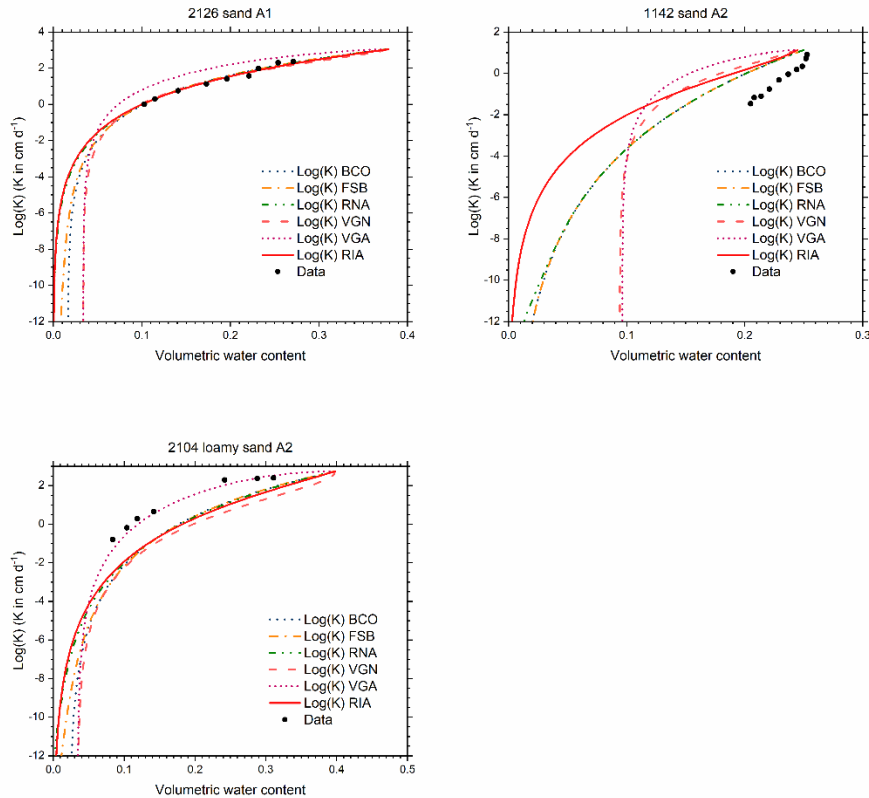
644

645   Figure C6. Conductivity data and conductivity curves derived from the retention curves of

646   Fig. C2 according to six parameterizations for selected UNSODA soils with Twarakavi et al.'s

647   (2010) A1 or A2 classification.
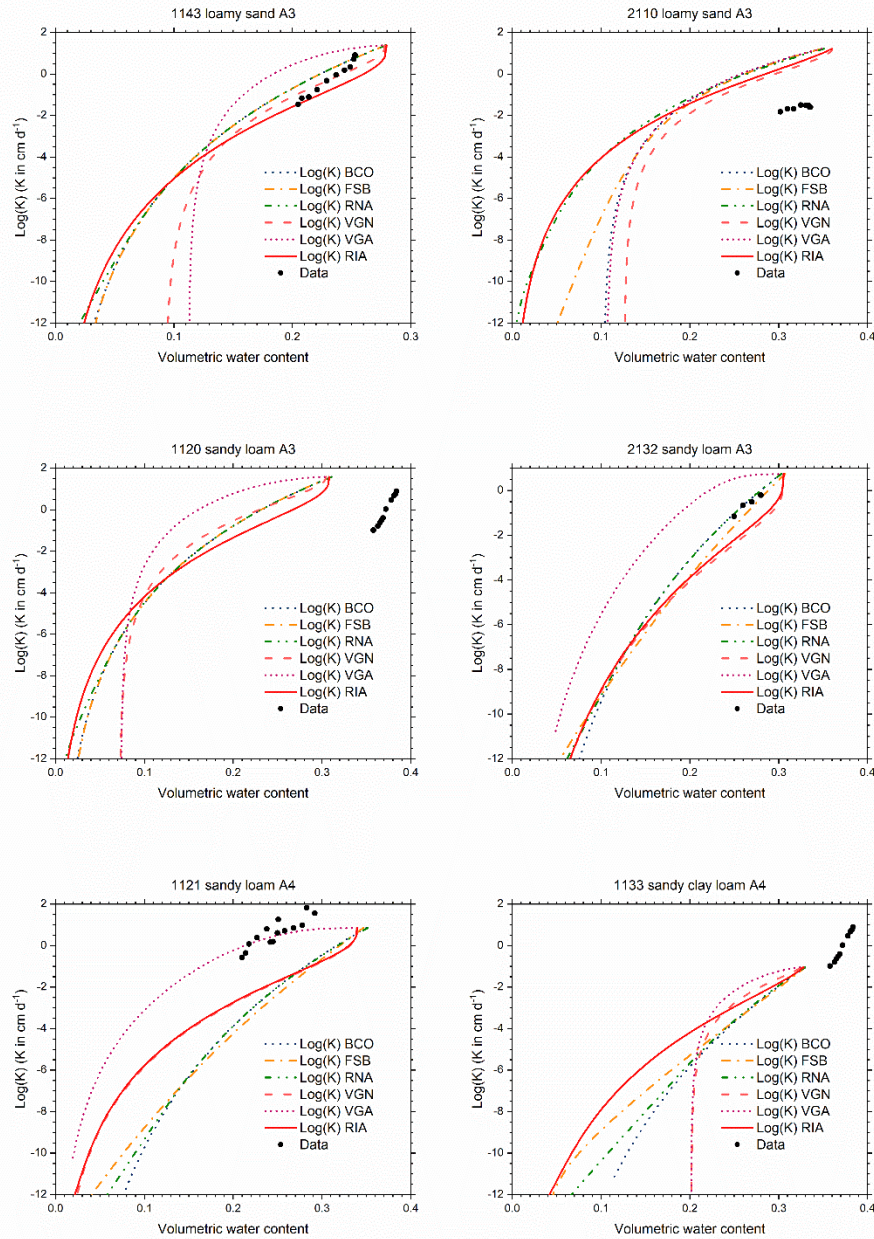
648

649   Figure C7. Conductivity data and conductivity curves derived from the retention curves of

650   Fig. C3 according to six parameterizations for selected UNSODA soils with Twarakavi et al.'s

651   (2010) A3 or A4 classification.
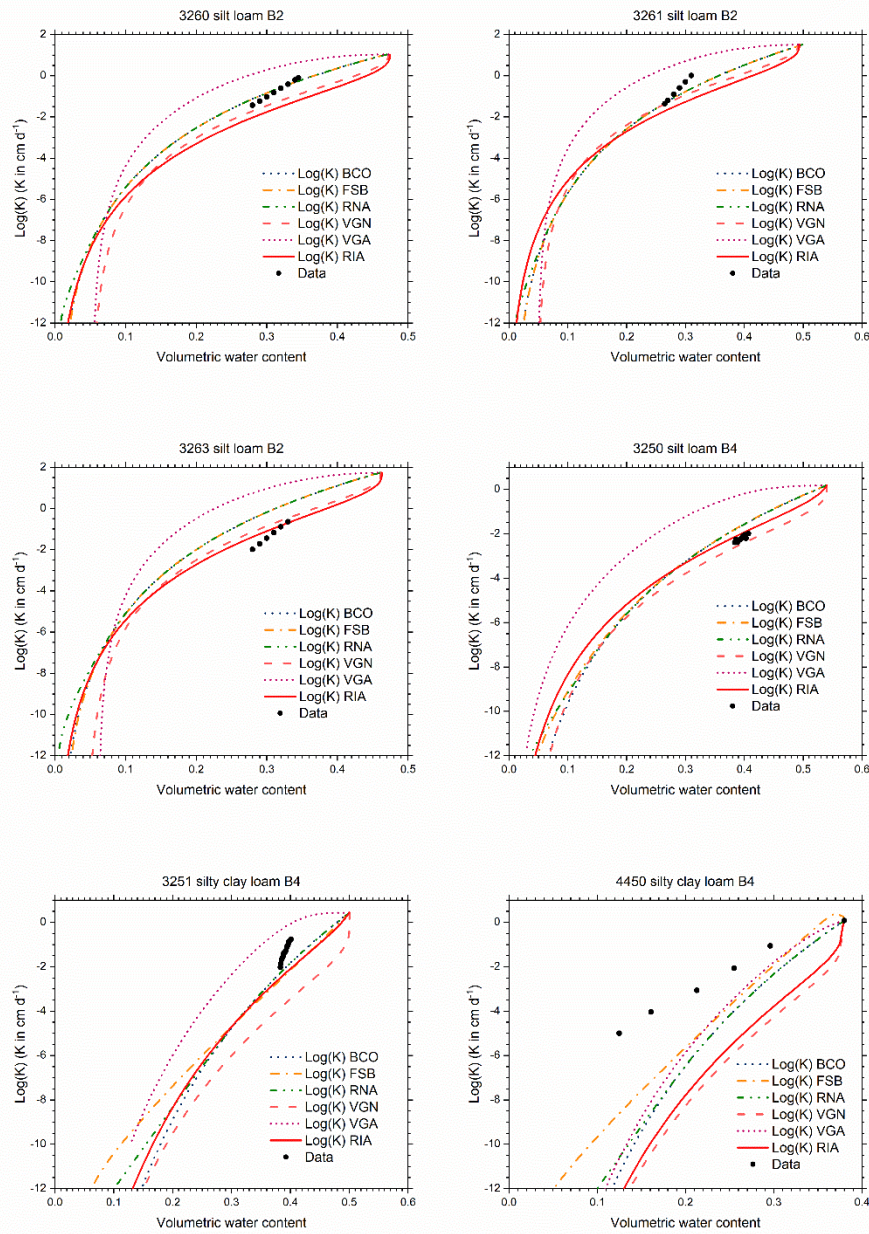
652

653   Figure C8. Conductivity data and conductivity curves derived from the retention curves of

654   Fig. C4 according to six parameterizations for selected UNSODA soils with Twarakavi et al.'s

655   (2010) B2 or B4 classification.
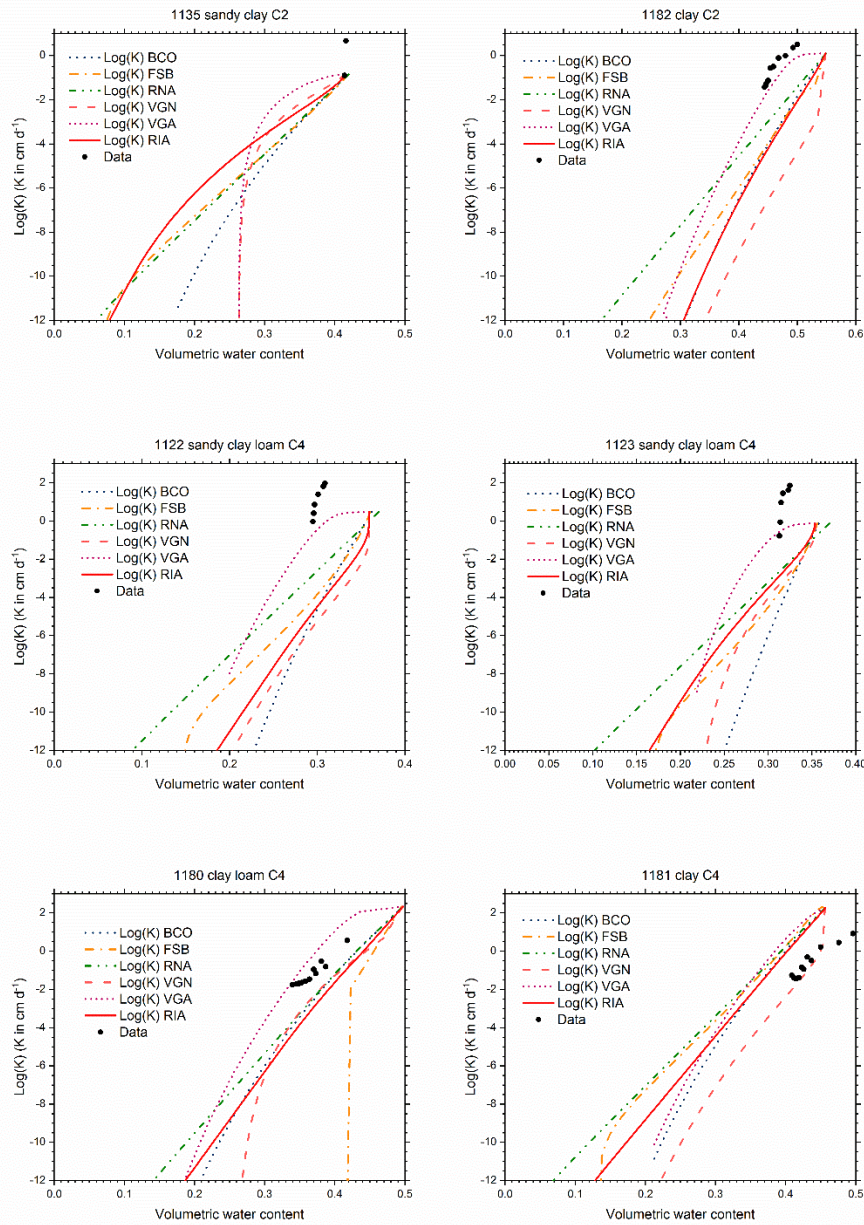
656

657   Figure C9. Conductivity data and conductivity curves derived from the retention curves of

658   Fig. C5 according to six parameterizations for selected UNSODA soils with Twarakavi et al.'s

659   (2010) C2 or AC4 classification.

660
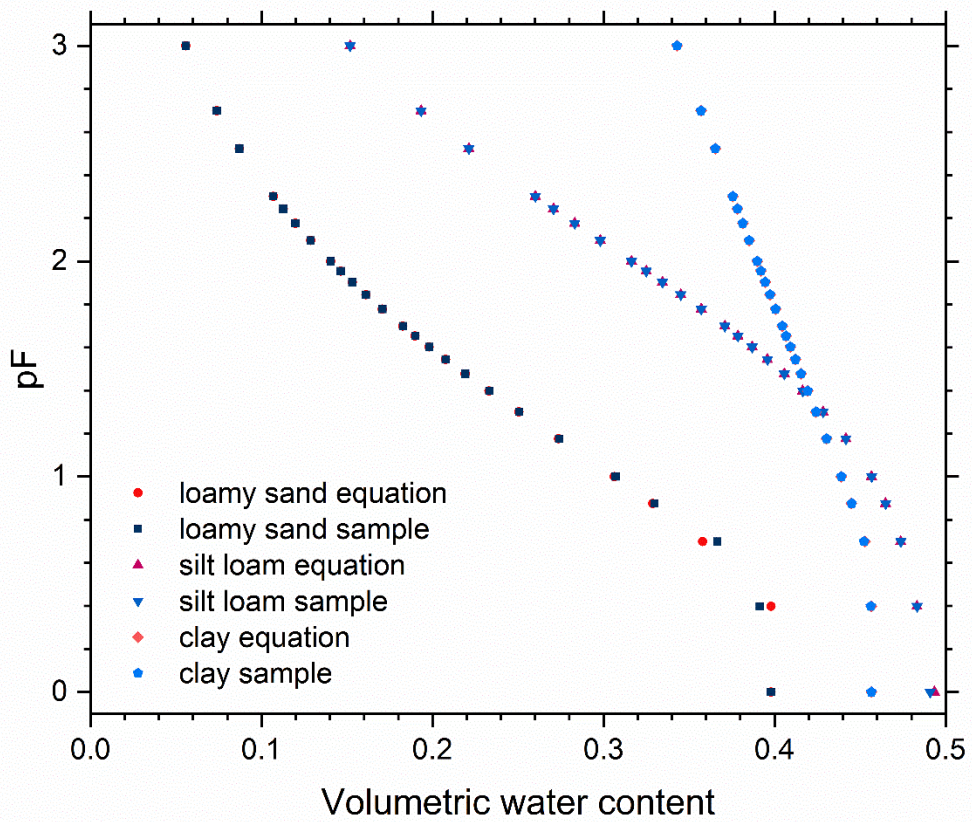
Figure C10. Soil water retention points calculated from RIA parameterizations for loamy

sand (UNSODA identifier 2104, classification according to Twarakavi et al. (2010) A4), silt

loam (3261, B2), and clay (1181, C4). The points were either calculated directly for the

given pF value ('equation'), or by calculating the average water content in a sample of 5.0

cm height at hydrostatic equilibrium, with the matric potential at the center of the sample

corresponding to the indicated pF value ('sample'). N.B. The data points for zero matric

potential were plotted at pF = 0 instead of pF = $-\infty$.

668

Author contributions

669

670

671 GdR developed the new parameterization, assisted by RM. GdR identified the 21 soils from

672 the UNSODA database and designed the model test. JM developed the SCE code for

673 parameter identification. GdR coded the shell around the SCE core to make it suitable for

674 fitting various SWRC parameterizations. GdR collected the weather data and generated the

675 weather records. GdR and RM carried out the paramter fitting and the Hydrus–1D

676 simulations. GdR wrote the manuscript with contributions from JM and RM.

677

Competing interests

678

679

680 GdR is a member of the HESS Editorial Board.

References

681 Assouline, S., and Or, D.: Conceptual and parametric representation of soil hydraulic

683   properties: a review, Vadose Zone J., doi: 10.2136/vzj2013.07.0121, 2013.

684 Assouline, S., Tessier, D., and Bruand, A.: A conceptual model of the soil water retention

685   curve, Water Resour. Res., 34, 223–231, 1998.

686 Bittelli, M., and Flury, M.: Errors in water retention curves determined with pressure plates,

687   Soil Sci. Soc. Am. J., 73, 1453–1460, doi: 10.2136/sssaj2008.0082, 2009.

688 Bradley, R. S.: Polymolecular adsorbed films. Part 1. The adsorption of argon on salt crystals

689   at low temperatures, and the determination of surface fields, J. Chem. Soc.

690   (Resumed), 1467–1474, doi: 10.1039/JR9360001467, 1936.

691 Brooks, R. H., and Corey, A. T.: Hydraulic properties of porous media, Hydrology Paper No.

692   3, Colorado State University, 1964.

693 Campbell, G. S., and Shiozawa, S.: Prediction of hydraulic properties of soils using particle–

694   size distribution and bulk density data, in: Proceedings of the international

695   workshop on indirect methods for estimating the hydraulic properties of

696   unsaturated soils, Riverside, California, Oct. 11–13, 1989, edited by: van Genuchten,

697   M. Th., Leij, F. J., and Lund, L. J.editors, Univ. California, Riverside, CA, U.S.A., 317–

698   328, 1992.

699 Cornelis, W. M., Khlosi, M., Hartmann, R., Van Meirvenne, M., and De Vos, B.: Comparison of

700   unimodal analytical expressions for the soil–water retention curve, Soil Sci. Soc. Am.

701   J. 69, 1902–1911, doi: 10.2136/sssaj2004.0238, 2005.

702 Durner, W.: Hydraulic conductivity estimation for soils with heterogeneous pore structure,

703   Water Resour. Res., 30, 211–223, 1994.

704   Fayer, M. J., and Simmons, C. S.: Modified soil water retention function for all matric

705   suctions, Water Resour. Res., 31, 1233–1238, 1995.

706   Fredlund, D. G., and Xing, A.: Equations for the soil–water characteristic curve, Can. Geotech.

707   J., 31, 521–532, 1994.

708   Fuentes, C., Haverkamp, R., Parlange, J. –Y., Brutsaert, W., Zayani, K., and Vachaud, G.:

709   Constraints on parameters in three soil–water capillary retention functions,

710   Transport in Porous Media, 6, 445–449, 1991.

711   Hillel, D.: Environmental soil physics, Academic Press, San Diego, CA, U.S.A., 1998.

712   Hutson, J. L. and Cass, A.: A retentivity function for use in soil-water simulation models, J. of

713   Soil Sci., 38, 105–113, 1987.

714   Iden, S. C., Peters, A., and Durner, W.: Improving prediction of hydraulic conductivity by

715   constraining capillary bundle models to a maximum pore size, Adv. Water Resour.

716   85, 86–92, doi: 10.1016/j.advwatres, 2015.09.005, 2015.

717   Ippisch, O., Vogel, H. –J., and Bastian, P.: Validity limits for the van Genuchten–Mualem

718   model and implications for parameter estimation and numerical simulation, Adv.

719   Water Resour., 29, 1780–1789, doi: 10.1016/j.advwatres.2005.12.011, 2006.

720   Khlosi, M., Cornelis, W. M., Douaik, A., van Genuchten, M. Th., and Gabriels. D.: Performance

721   evaluation of models that describe the soil water retention curve between saturation

722   and oven dryness, Vadose Zone J., 7, 87–96, doi: 10.2136/vzj2007.0099, 2008.

723   Khlosi, M., Cornelis, W. M., Gabriels, D., and Sin, G.: Simple modification to describe the soil

724   water retention curve between saturation and oven dryness, Water Resour. Res., 42,

725   W11501, doi: 10.1029/2005WR004699, 2006.

726 Klute, A.: Water retention: Laboratory methods, in: Methods of soil analysis. Part 1. Physical

727   and mineralogical methods. Second edition, edited by Klute, A., American Society of

728   Agronomy, Inc., Soil Science Society of America, Inc., Madison, WI, U.S.A., 635–662,

729   1986.

730 Kool, J. B., and Parker, J. C.: Development and evaluation of closed–form expressions for

731   hysteretic soil hydraulic properties, Water Resour. Res., 23, 105–114, 1987.

732 Koorevaar, P., Menelik, G., and Dirksen, C.: Elements of soil physics, Elsevier, Amsterdam,

733   The Netherlands, 1983.

734 Kosugi, K.: General model for unsaturated hydraulic conductivity for soils with lognormal

735   pore–size distribution, Soil Sci. Soc. Am. J., 63,270–277, 1999.

736 Kroes, J. G., van Dam, J. C., Bartholomeus, R. P., Groenendijk, P., Heinen, M., Hendriks, R. F. A.,

737   Mulder, H. M., Supit, I., and van Walsum, P. E. V.: SWAP version 4. Theory description

738   and user manual, Report 27480, Wageningen Environmental Research, Wageningen,

739   The Netherlands, 244 pp, doi: 10.18174/416321, 2017.

740 Leij, F. J., Russell, W. B., and Lesch, S. M.: Closed–form expressions for water retention and

741   conductivity data, Ground Water, 35, 848–858, 1997.

742 Liu, H. H., and Dane, J. H.: Improved computational procedure for retention relations of

743   immiscible fluids using pressure cells, Soil Sci. Soc. Am. J., 59, 1520–1524, 1995.

744 Madi, R., de Rooij, G. H., Mielenz, H., and Mai, J.: Parametric soil water models: a critical

745   evaluation of expressions for the full moisture range, Hydrol. Earth Syst. Sci. 22,

746   1193–1219, doi: 10.5194/hess-22-1193-2018, 2018.

747 Mualem, Y.: A new model for predicting the hydraulic conductivity of unsaturated porous

748   media, Water Resour. Res., 12, 513–522, 1976.

749   National Agricultural Library, UNSODA Database,

750   https://data.nal.usda.gov/dataset/unsoda-20-unsaturated-soil-hydraulic-database-

751   database-and-program-indirect-methods-estimating-unsaturated-hydraulic-

752   properties_134, last access 22 July 2020.

753   Nemes, A., Schaap, M. G., Leij, F. J., and Wösten, J. H. M.: Description of the unsaturated soil

754   hydraulic database UNSODA version 2.0., J. Hydrol., 251, 152–162, doi:

755   10.1016/S0022-1694(01)00465-6, 2001.

756   PC-progress: https://www.pc-progress.com/en/Default.aspx?hydrus-1d, last access: 22

757   July 2020.

758   Peters, A.: Simple consistent models for water retention and hydraulic conductivity in the

759   complete moisture range, Water Resour. Res., 49, 6765–6780, doi:

760   10.1002/wrcr.20548, 2013.

761   Peters, A., Durner, W., and Wessolek, G.: Consistent parameter constraints for soil hydraulic

762   functions, Adv. Water Resour., 34, 1352–1365, doi:

763   10.1016/j.advwatres.2011.07.006, 2011.

764   Rossi, C., and Nimmo. J. R.: Modeling of soil water retention from saturation to oven

765   dryness, Water Resour. Res., 30, 701–708, 1994.

766   Rudiyanto, Minasny B., Shah, R. M., Setiawan, B. I., and van Genuchten, M. Th.: Simple

767   functions for describing soil water retention and the unsaturated hydraulic

768   conductivity from saturation to complete dryness, J. Hydrol., 588, 125041, doi:

769   10.1016/j.jhydrol.2020.125041, 2020.

770   Schaap, M. G., and van Genuchten, M. Th.: A modified Mualem–van Genuchten formulation

771   for improved description of the hydraulic conductivity near saturation, Vadose Zone

772   J. 5, 27–34, doi: 10.2136/vzj2005.0005, 2006.

773   Schneider, M, and Goss, K. –U.: Prediction of the water sorption isotherm in air dry soils,

774   Geoderma, 170, 64–69, doi: 10.1016/j.geoderma.2011.10.008, 2012.

775   Šimůnek, J., and Bradford, S. A.: Vadose zone modeling: Introduction and Importance,

776   Vadose Zone J., 7, 581–586, doi: 10.2136/vzj2008.0012, 2008.

777   Šimůnek, J., Šejna, M., Sait., H., Sakai, M., and van Genuchten, M. Th.: The HYDRUS–1D

778   software package for simulating the one–dimensional movement of water, heat, and

779   multiple solutes in variably–saturated media, Version 4.17, Dept. Env. Sci., Univ.

780   Calif., Riverside, CA, U.S.A., 2013.

781   Šimůnek, J, van Genuchten, M. Th., and Šejna, M.: Recent developments and applications of

782   the HYDRUS computer software packages, Vadose Zone J., doi:

783   10.2136/vzj2016.04.0033, 2016.

784   Twarakavi, N. K. C., Šimůnek, J., and Schaap, M. G.: Can texture–based classification

785   optimally classify soils with respect to soil hydraulics?, Water Resour. Res. 46,

786   W01501, doi:10.1029/2009WR007939, 2010.

787   van Genuchten, M. Th.: A closed–form equation for predicting the hydraulic conductivity for

788   unsaturated soils, Soil Sci. Soc. Am. J., 44, 892–898, 1980.

789   Vogel, T., van Genuchten, M. Th., and Cislerova, M.: Effect of the shape of the soil hydraulic

790   functions near saturation on variably–saturated flow predictions, Adv. Water

791   Resour., 24, 133–144, 2001.

792   Wang, Y., Jin, M., and Deng, Z.: Alternative model for predicting soil hydraulic conductivity

793   over the complete moisture range, Water Resour. Res., 54, 6860–6876, doi:

794   10.1029/2018WR023037, 2018.

795   Wang, Y., Ma, J., and Huade, G.: A mathematically continuous model for describing the

796   hydraulic properties of unsaturated porous media over the entire range of matric

797   suctions. J. Hydrol,. 541, 873–888, doi: 10.1016/j.jhydrol.2016.07.046, 2016.

798   Weber, T. K. D., Durner, W., Streck, T., and Diamantopoulos, E.: A modular framework for

799   modeling unsaturated soil hydraulic properties over the full moisture range, Water

800   Resour. Res., 55, doi: 10.1029/2018WR024584, 2019.

801   Zurmühl, T., and Durner, W.: Determination of parameters for bimodal hydraulic functions

802   by inverse modeling, Soil Sci. Soc. Am. J., 62, 874–880, 1998.

803